Ph.D. Dissertation of Engineering

Radiation exposure reduction effect model in urban street and its application for decision making with trees

도심 보행자의 복사노출 저감평가 모델과
수목을 이용한 저감계획에서의 의사결정

August 2019

Graduate School of Seoul National University

Interdisciplinary Program in Landscape Architecture

Chae Yeon Park

Radiation exposure reduction effect model in urban street and its application for decision making with trees

Advisor: Dong Kun Lee

A dissertation submitted in partial fulfillment of the requirements for the Degree of Doctor of Philosophy in Interdisciplinary Program in Landscape Architecture in Seoul National University

August 2019

Chae Yeon Park

Approved by Thesis Committee

Chair	_____	(Seal)
Vice Chair	_____	(Seal)
Examiner	_____	(Seal)
Examiner	_____	(Seal)
Examiner	_____	(Seal)

Publications

Please note that Chapter 1-3 of this dissertation proposal were written as stand-alone papers (see below), and therefore there is some repetition in the methods and results.

CHAPTER 1

Park, CY., Lee, DK., Krayenhoff. E., Heo, HK., Ahn, S., Asawa, T., Murakami. A., Kim, HG., 2018. A multilayer mean radiant temperature model for pedestrians in a street canyon with trees. *Building and Environment.* 141, 298-309.

CHAPTER 2

Park, CY., Lee, DK., Krayenhoff. E., Heo, HK., Hyun, JH., Oh, K., Park, TY. 2019. Variations in pedestrian mean radiant temperature based on the spacing and size of street trees. *Sustainable Cities and Society.* 48, 1-9.

CHAPTER 3

Park, CY., Yoon, EJ., Lee, DK., Thorne, JH. Optimal multi-strategies modeling reveals a range of urban heat risk reduction options that integrate four heat exposure mitigation strategies, *Science of the Total Environment.* (Major revision)

Table of Contents

List of Figures

List of Tables

Abstract

Radiation exposure reduction effect model in urban street and its application for decision making

Chae yeon Park
Interdisciplinary Doctoral Program in Landscape Architecture
Graduate School, Seoul National University
Supervised by Professor Dong Kun Lee

Urban heat island and climate change have increased urban heat and threatened public health. Most streets are made of impervious surfaces and little vegetation. Also, cars and buildings are anthropogenic heat sources. Consequently, urban planners are considering heat mitigation strategies to prevent further increases in urban heating on streets. Critically, pedestrian thermal exposure depends on several factors in addition to air temperature, in particular the radiant environment in urban street canyons.

Several strategies have been studied for reducing radiation exposure of pedestrian. Among them, street tree is a well-known strategy to effectively reduce radiant heat by shade effect. But, decision makers such as urban planners do not know how much radiation is reduced by their decision about reducing radiation exposure. And it is difficult to know which options are the most effective for improving street thermal environment. Therefore, this

study aims to develop a decision making support tool that determines the effective radiation exposure reduction plans with trees.

The study developed a model to estimate the pedestrian radiant heat load that is suitable for urban street with varying tree and building design. The model simulates shortwave and longwave radiation exchange for each urban element and area-weighted view factors, then finally obtains mean radiant temperature (MRT) of pedestrians on the sidewalk.

Using this estimation model, the study examined the variation of MRT depending on the tree design parameters (e.g., tree size and interval). The results showed that as the tree interval decreased, MRT reduction was increased exponentially by small trees, while MRT reduction was increased linearly by large trees. Based on this results, decision maker can identify MRT reduction effect of trees and select most appropriate tree design parameters.

A variety of MRT reduction strategies can be applied to one site. To reflect a real world, the study proposed a multi-strategies combination model. To find the effective combination plans consisting of tree, grass, albedo reduction of building walls and sidewalk, the objective functions were set: maximizing MRT reduction and minimizing the cost. The model provide a wide range of alternatives to satisfy these objectives, allowing decision makers to select plan tailored to their preference or site condition.

This study seeks to develop useful decision support tool for urban planner by providing quantitative effect of tree and a range of options with cost-effective strategies combination. This will provide insights for sustainable

urban planning by designing thermal-friendly streets with tree.

Keywords: Urban heat island, tree planning, Mean radiant temperature, Optimization, shading effect

Student Number: 2017-37831

I. Introduction

Urban areas have been warming as a result of climate change and urbanization (Stewart & Oke, 2012). This phenomenon has a negative effect on people livings in these areas, as the increased heat flux, causes discomfort, lower productivity, and heat-related diseases (Brown, Vanos, Kenny, & Lenzholzer, 2015; J. Wang, Huang, Fu, & Atkinson, 2015). People who walk around outdoor streets are particularly vulnerable to increased urban heating and heat stress. Little vegetation, impermeable surfaces, and anthropogenic heat sources enhance the heat in street canyons; this is transferred to pedestrians. Consequently, urban planners are considering heat mitigation strategies to prevent further increases in urban heating on streets.

Many heat mitigation strategies are used in existing urban areas, including converting impervious surfaces to cool or permeable surfaces, providing water bodies, increasing the amount of vegetation, and green infrastructure (Dimoudi et al., 2014; L. Kong et al., 2017; Rizwan, Dennis, & Liu, 2008; Rosso et al., 2018; Takebayashi, Kimura, & Kyogoku, 2014; Tominaga, Sato, & Sadohara, 2015; Zoras, Tsermentselis, Kosmopoulos, & Dimoudi, 2014). Converting surfaces to high albedo surfaces have been recognized as cooling strategies in urban street (Alchapar, Correa, & Cantón, 2014; Zoras et al., 2014). However, latest research found high albedo surfaces could reflect radiation to the pedestrian, which resulted in increasing heat stress (Erell, Pearlmutter, Boneh, & Kutiel, 2014; Lee & Mayer, 2018b). Water and green

infrastructure play urban cool islands by reducing sensible heat using conduction, radiation blocking and providing latent heat (Y. C. Chen, Tan, Wei, & Su, 2014; Du et al., 2016; Feyisa, Dons, & Meilby, 2014; F. Kong, Yin, James, & He, 2014; R. Sun, Chen, Chen, & Lü, 2012).

In the pedestrian level, radiation heat flux is the major component to increase heat stress. Many researchers have been used mean radiant temperature (MRT) to assess the meteorological component of heat stress (De & Mukherjee, 2017; J. Huang, Cedeño-Laurent, & Spengler, 2014; Kántor, Chen, & Gál, 2018; Kántor, Gál, Gulyás, & Unger, 2018; Klemm, Heusinkveld, Lenzholzer, & van Hove, 2015; Lindberg & Grimmond, 2011; Oliveira, Andrade, & Vaz, 2011; Taleghani, Sailor, Tenpierik, & van den Dobbelsteen, 2014); this metric integrates radiation flux densities emitted and reflected from surrounding surfaces and from the sun and sky, and quantifies the amount of radiative energy incident on a pedestrian (Matzarakis, Rutz, & Mayer, 2010). Many factors affect pedestrian's MRT in urban streets, including urban form, material properties, and implementation of green infrastructure, which are involved in radiation transfer process. In this respect, green infrastructure that mitigates urban radiation flux by generating shade on the ground and wall and converting wall or pavement material that controls reflectance can be good solutions to reduce MRT (Abreu-Harbich, Labaki, & Matzarakis, 2015; Lee & Mayer, 2018b; Lindberg & Grimmond, 2011).

Among several strategies for reducing pedestrian's MRT, tree is a popular strategy due to their shading effect. Tree shade reduced solar radiation up to

76-93 % during summer (Abreu-Harbich et al., 2015; Holst & Mayer, 2011). Although many previous studies have found the MRT reduction effect of tree, there is no available information for supporting decision making in urban plan. For example of street tree, researchers have not provided specific design parameters trees that can be applied to urban planning. Some studies have measured the reduction of urban heat due to trees at specific field study sites (D. Armson, Stringer, & Ennos, 2012; Klemm et al., 2015; Lee, Holst, & Mayer, 2013). However, these results are limited to the study site and are difficult to apply to other areas. Other studies have used numerical simulations to confirm that larger and denser trees are more effective at mitigating urban heat. The heat mitigation effect of the tree became greater as far as the leaf area index became larger (E. S. Krayenhoff, Christen, Martilli, & Oke, 2014; Morakinyo & Lam, 2016; Ryu, Bou-Zeid, Wang, & Smith, 2016) and the tree height became taller (E. S. Krayenhoff et al., 2014; Ryu et al., 2016). These results are also difficult to apply to urban planning because the urban planner must select trees within limited space and budget, which are relatively fixed parameters. When provided with a range of options and evidence for optimal tree planting intervals, planners can work within their given parameters to make the best decision.

In a real world urban planning, several strategies are considered at the same time. And combining multiple strategies could result in different effects (E. Scott Krayenhoff, Moustaoui, Broadbent, Gupta, & Georgescu, 2018), which is called as combination effect in this study. However, many studies

focused on single strategy (Dimoudi et al., 2014; Djedjig, Bozonnet, & Belarbi, 2016; Napoli, Massetti, Brandani, Petralli, & Orlandini, 2016; Oliveira et al., 2011) and this results could make decision makers underestimate or overestimate the effect of multiple strategies. In addition, decision makers must consider the cost effectiveness in order to provide maximum effect within a limited budget. Therefore, the new decision support tool for considering multi-objective and multi-strategies in order to reduce pedestrian's MRT and researchers should provide a wide range of optimal options that contains cost-effective strategies combination.

For providing these decision support information, estimation of MRT reduction strategies should be prioritized. One of the reason for lack of information is the lack of the simulation model to assess the MRT reduction effect. Because many factors affect MRT, each research requires an MRT simulation model that is appropriate for our purposes. However, no currently available model can evaluate pedestrian's MRT, focusing on both the urban street canyon and diverse strategies including street tree, and grass, with simple input data.

The purpose of this study is evaluating the MRT reduction effect of critical strategies in urban street and providing urban design parameters information. I selected street tree (chapter 2 and 3), grass (greenway along the sidewalk) (chapter 3), and low albedo material (chapter 3) as the MRT reduction strategies (Fig. 1). For assessing the MRT, I developed multi-layer MRT which is an effective simulation model in urban street with trees (chapter 1).

In chapter 2, focusing on the street tree, variations of MRT reduction of street trees with critical design variables: tree size and interval. In chapter 3, focusing on the strategies combination and cost-effectiveness, I developed optimal multi-strategies model that provided a range of MRT reduction options.

The results of this study fill the gap between the research on the cooling effect and urban planning to mitigate radiation exposure by providing data: variation of MRT reduction depending on tree size and interval, and series of strategies combination.

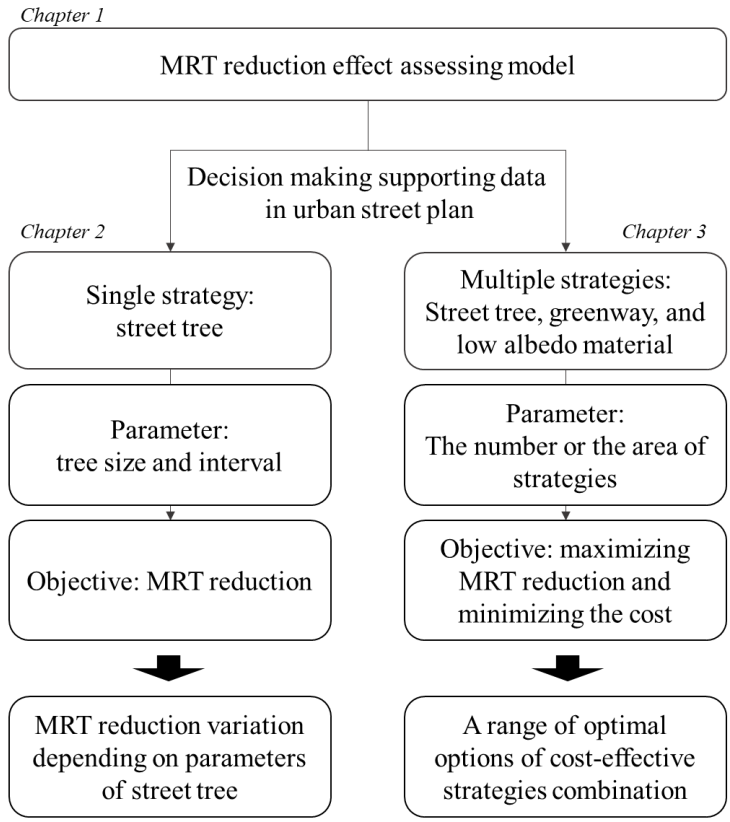

Fig. 1. Outline of the study and its objectives.

II. CHAPTER 1: A multilayer mean radiant temperature model for pedestrians in a street canyon with trees

2.1. Introduction

Urban heating from development and climate change is projected to modify pedestrians' energy balance and worsen thermal comfort (L. Kong et al., 2017). Many researchers used mean radiant temperature (MRT) to assess the meteorological component of outdoor thermal comfort (De & Mukherjee, 2017; J. Huang et al., 2014; Kántor, Chen, et al., 2018; Kántor, Gál, et al., 2018; Klemm et al., 2015; Lindberg & Grimmond, 2011; Oliveira et al., 2011; Taleghani, Sailor, et al., 2014). MRT is one of the most important human bio-meteorological variables, especially for daytime in clear-sky summer days (Holst & Mayer, 2011; Lee et al., 2013; Lee, Mayer, & Chen, 2016; Lee, Mayer, & Schindler, 2014; Mayer, Holst, Dostal, Imbery, & Schindler, 2008). This metric integrates shortwave and longwave radiation flux densities emitted and reflected from the tree dimensional environment and quantifies the amount of radiative energy incident on a pedestrian (Holst & Mayer, 2011; Lee et al., 2013; Thorsson, Lindberg, Eliasson, & Holmer, 2007).

Many factors affect pedestrians' MRT in urban streets, including urban form, material properties, and implementation of green infrastructure (Lee & Mayer, 2016). Urban form can control sun exposure and shading, cause a significant effect on shortwave radiation flux densities, and determine

outdoor heat conditions (Holst & Mayer, 2011; Lee et al., 2013; Xuan, Yang, Li, & Mochida, 2016). For example, street orientation and aspect ratio are important microclimate modulators (Ali-Toudert & Mayer, 2006; De & Mukherjee, 2017; Holst & Mayer, 2011). Modifying pavement albedo can reduce surface temperature (Alchapar et al., 2014; Zoras et al., 2014), but may also be problematic on pedestrian heat balance (Erell et al., 2014), whereas the application of cool materials implemented may improve urban climate (E. Scott Krayenhoff & Voogt, 2010; Rosso et al., 2018). Green structures mitigate urban radiation flux by generating shade on the ground and walls (Lee et al., 2016; Lindberg & Grimmond, 2011). Among these modifications, planting trees is a good solution because trees serve the ecosystem in a variety of ways in addition to their cooling benefits (Jamei & Rajagopalan, 2017; L. Kong et al., 2017). Many studies confirmed that trees can influence urban microclimates and reduce the radiation heat flux absorbed by a person because of their reflection, transmission, and absorption of shortwave radiation, which is called the shading effect (Abreu-Harbich et al., 2015; Holst & Mayer, 2011; Lee et al., 2013).

A previous research suggested that the most important variables for determining a tree's cooling effects are size, leaf area index or density, and location (E. S. Krayenhoff et al., 2014; Morakinyo & Lam, 2016; Redon, Lemonsu, Masson, Morille, & Musy, 2016; Ryu et al., 2016; Takebayashi et al., 2014). Wider trees with taller crowns can absorb more radiation (E. S. Krayenhoff et al., 2014; Ryu et al., 2016; Takebayashi et al., 2014). The leaf

area index (LAI, [m^2/m^2]) and the leaf area density (LAD, [m^2/m^3]) also indicate the leaves' photosynthetic capacity, which is strongly related to a tree's capacity to provide shade and reduce daytime MRT. In particular, LAD reflects the leaves' volumetric density and can be used to determine radiation attenuation (Iio, Kakubari, & Mizunaga, 2011). Lastly, location includes the spacing between trees, spacing between trees and buildings, and direction of the tree row (Morakinyo & Lam, 2016; Redon et al., 2016; Ryu et al., 2016). The effect of a tree varies depending on the elements that surround it; hence, its relative location must be considered.

Many factors affect MRT; thus, this study requires an MRT simulator that is appropriate for the purposes. ENVI-met, SOLWEIG, and RayMan are the best-known MRT simulators that consider 3D urban morphology. They are highly-cited, indicating demand for tools to assess spatially-variable human bio-meteorological impacts in urban areas (Hondula et al., 2017; Kántor, Gál, et al., 2018; Lee et al., 2016). The latest version of ENVI-met can simulate MRT in complex urban settings (Lee et al., 2016). However, it focuses on the other meteorological variables (i.e. air temperature, wind speed, humidity) as well as MRT. And those three simulators simplify calculation for diffuse shortwave and longwave radiation using the sky view factor to obtain MRT of all complex 3D regions. (Ali-Toudert & Mayer, 2006; Lindberg, Holmer, & Thorsson, 2008; Matzarakis et al., 2010). RayMan is not appropriate for highly heterogeneous urban areas (Lee & Mayer, 2016). No currently available model can evaluate pedestrians' MRT, focusing on both the urban

street canyon and trees, with an accurate radiation transfer process. While previous simulators are appropriate for the estimation of MRT of a study area with CAD-based shape files and digital elevation models (Lindberg & Grimmond, 2011; Matzarakis et al., 2010), they are not suitable for comparing pedestrian MRT values that vary according to MRT mitigation strategies because of their complexity of input data and improper capturing of multiple radiation physical processes.

An urban multilayer radiation model was first introduced by Martilli et al. (Martilli, Clappier, & Rotach, 2002) and re-developed by Krayenhoff et al. (E. S. Krayenhoff et al., 2014) with (Monte Carlo) ray tracing to include urban trees. This study develops a similar multilayer MRT (MMRT) model for estimating pedestrians' radiation heat flux in a street canyon. The proposed model is two-dimensional (2D) and requires only simple input data, but applies to complex urban streets with diverse building and tree heights and densities caused by the multilayer geometry and flexible Monte Carlo ray tracing (MCRT) approach. These multilayer systems are novel in their ability to consider the vertical heterogeneity of urban areas. Using a multilayer system, the study develops a new MRT model that encapsulates the radiation transfer process in complex urban streets at the microscale. The input data are designed to consider major MRT control factors regarding urban form, pavement, and trees. The results can be used to design streets for improved thermal comfort when used with air temperature, humidity, and wind speed.

2.2. Methods

2.2.1. Research flow

This study focuses on developing an MMRT model based on a multilayer urban radiation model that divides the vertical domain into layers and enables the consideration of heterogeneous vertical buildings and vegetation layers (E. S. Krayenhoff et al., 2014). The study evaluates this model using view factors and multilayer variables (i.e., probability density profiles of buildings and trees). The view factor is the fraction of energy leaving one surface, which reaches the other surface and is calculated with an analytical computation. However, analytically determining the complex urban geometry, especially with tress, is difficult (Overby, Willemsen, Bailey, Halverson, & Pardyjak, 2016). Hence, the study uses MCRT to calculate the view factors in a street canyon within trees and compare them with the analytical view factors for verification. From this comparison, this study determines the number of rays required for good results without excess computation. Second, this study confirms the suitability of the probability density representation of complex urban streets. This model uses a density profile; hence, MRT can be calculated in a single process even if the street canyon site contains many diverse buildings and tree heights. After validation, this study conducts sensitivity tests using tree variables (i.e., tree height and LAD). Fig. 2 presents a complete flow chart of our methodology.

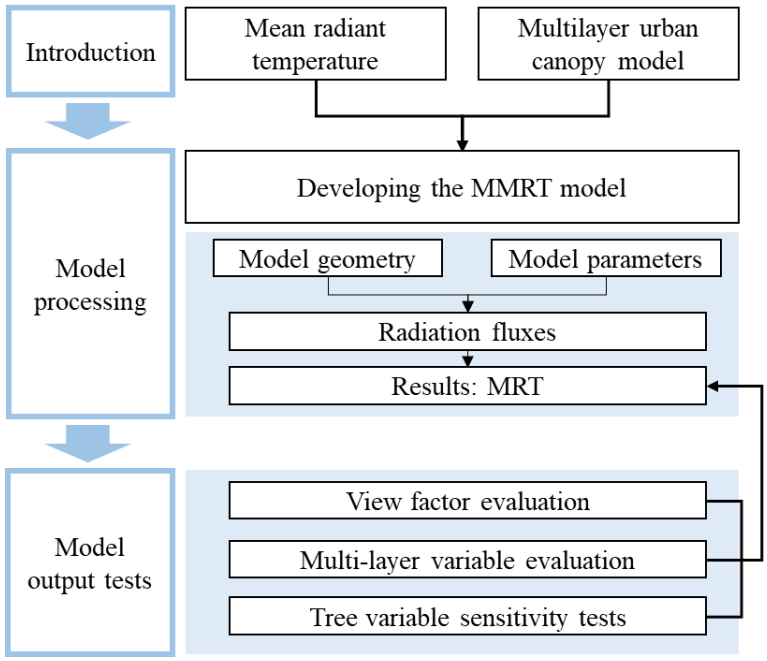

Fig. 2. Flowchart of our research process.

2.2.2. Developing the MMRT model

2.2.2.1. Model geometry

This model is focused on pedestrians' MRT in a street canyon; thus, this study consider a domain that includes an infinitely long block within a road in the middle and buildings on two sides. It is conceptualized with equal road width and randomly ordered building height. The model domain is composed of six elements: building walls, roofs, sidewalks, road, street trees, and the sky. The elements in pairs are divided into sunlit and shaded. This 2D (cross-section) domain is the result of compressing the 3D urban block (Fig. 3). This

study divides the vertical component of buildings (walls and roofs) and tree's LADs into 10 layers (iz = 1, 2, 3…10) to reflect a real urban street geometry and consider tree-building radiation interactions. The vertical thicknesses of the building and tree layers are denoted as Δz and Δzt, respectively. This study then designated a building profile value and a tree LAD in each layer. This density profile indicates the probability that the element exists in the 3D urban canyon (E. S. Krayenhoff et al., 2014).

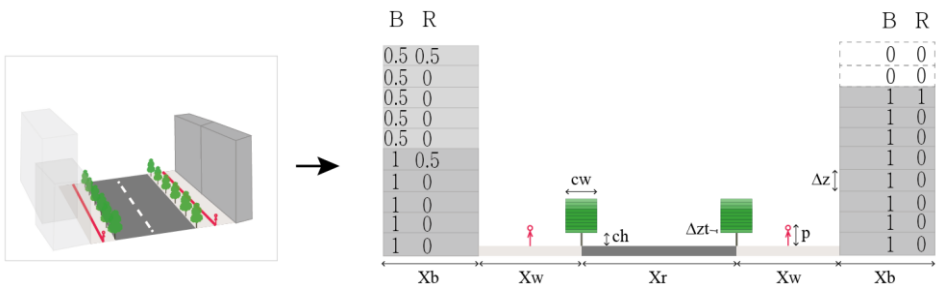

Fig. 3. 2D model domain (right) derived from the compression of the 3D urban canyon street (left). (Xb: building width, Xw: sidewalk width, Xr: road width, ch: tree trunk height, cw: tree crown width, p: pedestrian height, $\Delta \boldsymbol{z}$: vertical layer thickness of building, $\Delta \boldsymbol{zt}$: vertical layer thickness of tree).

In the domain, two building columns with widths and density profile matrices B (shaded areas) and SB (sunlit areas) flank two sidewalks and one road, and the widths of which are denoted by Xw and Xr, respectively. The roof probability density profile can also be defined from the building (wall) probability density profile as matrix R. For example, if all buildings' heights are 40 m, and Δz is 5 m, matrix B can be defined as [1 1 1 1 1 1 1 1 0 0], and matrix R becomes [0 0 0 0 0 0 0 1 0 0]. A detailed explanation on B and R can be found in Martilli et al. (2002). The trees are in two rows with the leaf area profile density matrix V. V is defined as the LAD matrix that is the

sum of the leaf area per tree row volume. In this study, the tree rows are limited to the crown boxes ($cw * (\Delta zt * 10)$), where cw is the width. This study assumes the standing position of pedestrians, whose heights are p walk on the middle of the sidewalks on the shaded and sunlit sides of the canyon. Therefore, pedestrians are $Xw/2$ m from the trees.

2.2.2.2. Model parameters

The input data are classified into four classes: date and time, latitude and longitude, meteorological data, and geometric data. Date, time, latitude, and longitude are mainly used to calculate the solar angle and the solar irradiance. The meteorological data used to assess the surface temperature and the longwave radiation include air temperature, dew temperature, cloud fraction, and wind speed. The geometric data, including the widths and heights of buildings, road, sidewalks, and trees, are described in Section 2.2.1. The model parameters are listed in the Appendix, including the input data and the intermediate products of the model.

2.2.2.3. Model flow

The model must first calculate the incident and leaving shortwave and longwave radiation of each urban element. Then, it calculates the pedestrians' MRT using the emitted and reflected radiation from the elements to pedestrians and view factors (Fig. 4).

Our radiation calculation method is mainly derived from E. S. Krayenhoff et al. (2014), although the geometry of the urban elements, simulated global radiation, and surface temperature differ. The model focuses on pedestrians; hence, additional direct solar radiation and view factors are calculated for the pedestrians. Our simulation of the global radiation uses equations from Allen et al. (1998), and our surface temperature simulation uses equations from Matzarakis et al. (2010).

The model can be process with MATLAB. It is made of a function and sub functions for direct solar radiation K_{dir} and view factors $f_{E_i \to E_j}$

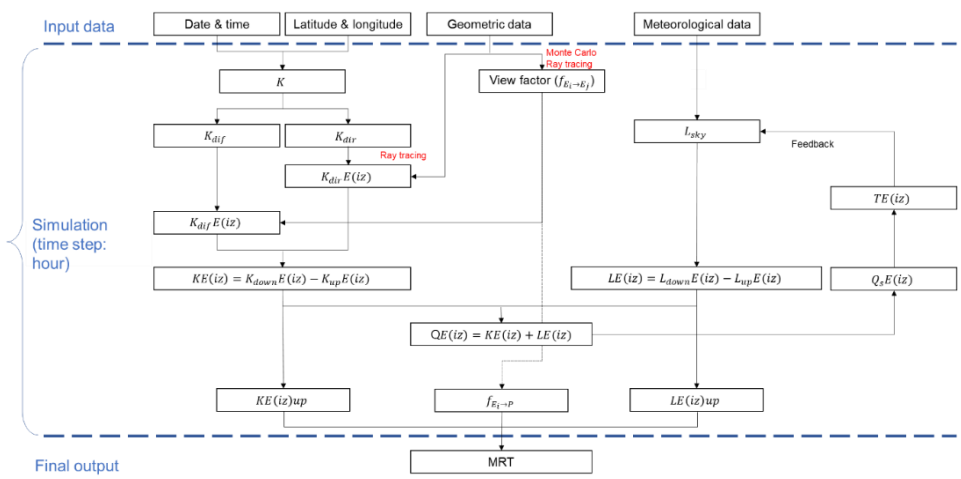

Fig. 4. Model flow. Please refer to Table A.1 for variable definitions.

2.2.2.4. Calculating radiation

2.2.2.4.1. Shortwave radiation

First, the model calculates the global and extraterrestrial shortwave radiation from the date, time, and cloud fraction (Allen et al., 1998). Second, the model divides it into direct and diffuse radiation using Eqs. (1)–(3) from the Erbs model (Erbs, Klein, & Duffie, 1982; W. Park, Kang, Park, Lee, & Song, 2012). This equation has better performance compared to other models, especially in Korea (Dervishi & Mahdavi, 2012; W. Park et al., 2012).

$$K^T = \frac{K}{K^O sin(^{\pi}/_2 - \theta)} \tag{1}$$

$$^{K_{dir}}/_K =$$

$$\begin{cases} 1.0 - 0.09K^T & K^T \leq 0.22 \\ 0.9511 - 0.1604K^T + 4.388K^{T2} - 16.638K^{T3} + 12.336K^{T4} & 0.22 < K^T \leq 0.80 \\ 0.165 & K^T \geq 0.80 \end{cases} \tag{2}$$

$$K = K_{dir} + K_{dif} \tag{3}$$

Direct shortwave radiation is the irradiance from the sky. Its direction varies based on time and location. Meanwhile, diffuse shortwave radiation comes down from every direction as it is scattered in the atmosphere. Our model uses ray tracing to calculate the direct shortwave radiation on urban elements. Bundle of rays with direct shortwave energy are evenly placed in the sky. The user defines the number of rays, each of which comes downward with a certain direction and step size. The ray direction is defined by the solar zenith, azimuth angle, and street orientation (E. S. Krayenhoff et al., 2014; Martilli et al., 2002) by Eq. (4):

$$\text{ray direction} = \text{atan}\left(\frac{\tan(\theta)}{\sin(\varphi - \chi)}\right). \tag{4}$$

As each ray descends, its energy is calculated at every step size. When the ray meets an urban element, that element intercepts and absorbs the ray's energy. When rays are intercepted, they lose their incident strength, which eventually decreases to zero. Specifically, when the rays are in layers of B, SB, and V, interception happens every ray step (Fig. 5).

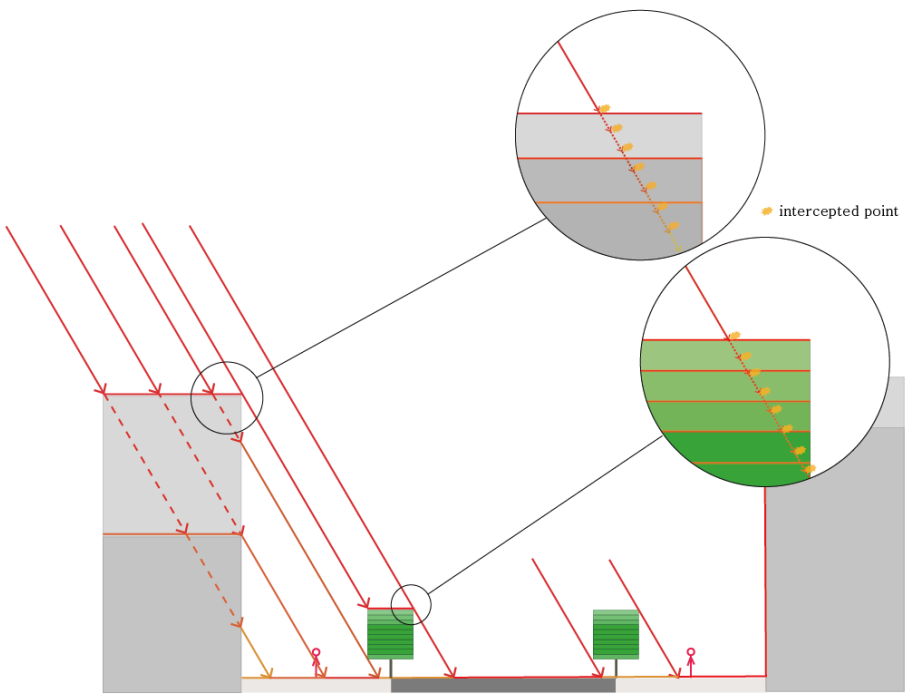

Fig. 5. Model geometries and solar radiation intercepted by urban elements.

The amount of energy intercepted depends on the element type. These equations come from E. S. Krayenhoff et al. (2014). Rays lose energy when they are by intercepted by urban elements. The lost energy of ray i at step j ($\Delta Ray_{i,j}$) is equal to the energy intercepted by urban elements. Therefore,

ray energy $Ray_{i,j}$ can be calculated by subtracting the lost energy from the previous step ray energy using Eq. (5). The element's intercepted energy at each ray step is expressed by Eqs. (6)–(9).

$$Ray_{i,j} = Ray_{i,j-1} - \Delta Ray_{i,j} \quad (5)$$

(Sunlit wall) $$\Delta SB_{i,j} = Ray_{i,j-1} SB(iz) = -\Delta Ray_{i,j} \quad (6)$$

(Roof) $$\Delta R_{i,j} = Ray_{i,j-1} R(iz) = -\Delta Ray_{i,j} \quad (7)$$

(Tree) $$\Delta V_{i,j} = Ray_{i,j-1}[1 - \exp(-K_{bs}\Omega V(iz)\Delta sf_i)] = -\Delta Ray_{i,j} \quad (8)$$

(Sidewalks, roads, pedestrians) $$\Delta E_{i,j} = Ray_{i,j-1} = -\Delta Ray_{i,j} \quad (9)$$

Δs is the 2D ray step size; therefore, the model can determine the corresponding 3D distance travelled by the ray by multiplying the ratio of 3D to 2D distance travelled (E. S. Krayenhoff et al., 2014), which is important for the accurate attenuation of radiation traveling through tree foliage layers. K_{bs} is the leaves' extinction coefficient, and Ω is the clumping factor (0–1, where 1 indicates a random distribution). This study sets K_{bs} and Ω to 0.5 (E. S. Krayenhoff et al., 2014). This study also assumes that sidewalks, roads, and pedestrians absorb all ray energy when they meet a ray. A pedestrian in sunlit makes a shadow on the sidewalk. Finally, the absorbed direct shortwave radiation can be calculated as follows using Eq. (10):

$$K_{dir}E(iz) = \frac{K_{dir}}{ni}\frac{\sum_{i,j}\Delta E_{i,j}}{AE(iz)} \quad (10)$$

AE(iz) is the area ratio of element E, and level iz is calculated as follows using Eqs. (11)–(16):

$$\mathrm{AB(iz)} = \left(\frac{z}{Xb+2Xw+Xr}\right) \mathrm{B(iz)} \quad (11)$$

$$\mathrm{AR(iz)} = \left(\frac{\mathrm{xb}}{Xb+2Xw+Xr}\right) \mathrm{R(iz)} \quad (12)$$

$$\mathrm{AT(iz)} = \left(\frac{\Omega*\Delta zt*\mathrm{Cw}}{\mathrm{Xb+2Xw+Xr}}\right) 2V(iz) \quad (13)$$

$$\mathrm{AW} = {}^{\mathrm{Xw}}/_{\mathrm{Xb} + 2\mathrm{Xw} + \mathrm{Xr}} \quad (14)$$

$$\mathrm{AR} = {}^{\mathrm{Xr}}/_{\mathrm{Xb} + 2\mathrm{Xw} + \mathrm{Xr}} \quad (15)$$

$$\mathrm{AP} = {}^{2}/_{\mathrm{Xb} + 2\mathrm{Xw} + \mathrm{Xr}} \quad (16)$$

The model must first obtain the view factors between the urban elements to calculate the diffuse shortwave radiation (H. Huang, Ooka, & Kato, 2005; Z.-H. Wang, 2014). View factors are needed to calculate the diffuse shortwave radiation, emitted longwave radiation, and reflection between the urban elements. Calculating the view factors between elements in complex urban areas is difficult using analytical methods (H. Huang et al., 2005). However, MCRT can determine any view factor, even in urban environments that include trees (Ryu et al., 2016).

The difference between MCRT and ray tracing for direct shortwave radiation is the ray direction. The model use a certain ray direction and start

point to calculate the direct shortwave radiation. In contrast, for the view factor calculation, the model provide the zenith angle with a random number and a random start point to each ray. The rays' zenith angle is $\cos^{-1}\sqrt{1-rand}$, where $rand$ is a random number between 0 and 1. The equations of the energy intercepted by the urban elements are the same as those used when calculating the direct shortwave radiation. Finally, the view factors are calculated using Eq. (17):

$$\mathrm{f}_{E(iz)\to E'(jz)} = \frac{1}{ni}\sum_{i,j}\Delta E'_{i,j}(jz) \tag{17}$$

This model uses an area-weighted view factor that accounts for the area ratio between sending and receiving elements, as Eq. (18) in E. S. Krayenhoff et al. (2014):

$$\mathrm{F}_{E(iz)\to E'(jz)} = f_{E(iz)\to E'(jz)}\left\{AE(iz)\Big/AE'(jz)\right\} \tag{18}$$

The diffuse shortwave radiation from the sky is absorbed by the urban elements. Therefore, the amount of diffuse shortwave radiation absorbed is obtained by multiplying the weighted view factors of the sky ($\mathrm{F}_{S\to P(iz)}$) using Eq. (19):

$$\mathrm{K}_{dif}E(iz) = \mathrm{K}_{dif}F_{S\to E(iz)} \tag{19}$$

The net shortwave radiation $KE(iz)$ is the amount of downward (incident) shortwave radiation $K_{down}E(iz)$ minus the amount of upward (leaving) shortwave radiation $K_{up}E(iz)$. $\mathrm{K}_{down}\mathrm{E(iz)}$ is composed of direct, diffuse,

and reflected shortwave radiation from other elements. For a building wall, the model follows Eq. (20) in Martilli et al. (2002) and E. S. Krayenhoff et al. (2014):

$$\mathrm{K}_{down}B(iz) = \mathrm{K}_{dir}B(iz) + F_{sky\to B(iz)}K_{dif} + \sum_{jz=1} F_{SB(jz)\to B(iz)}\alpha_B K_{net}SB(jz) + \sum_{jz=1} F_{R(jz)\to B(iz)}\alpha_R K_{net}R(jz) + F_{G\to B(iz)}\alpha_G K_{net}G(jz) + F_{W(jz)\to B(iz)}\alpha_W K_{net}W(jz) + \sum_{jz=1} F_{V(jz)\to B(iz)}\alpha_V K_{net}V(jz) \quad (20)$$

$K_{up}E(iz)$ denotes the reflected shortwave radiation from E(iz), which depends on its albedo by Eq. (21):

$$\mathrm{K}_{up}\mathrm{E(iz)} = \alpha_E\ \mathrm{K}_{down}\mathrm{E(iz)} \quad (21)$$

Therefore, KE(*iz*) can be calculated using Eq. (22):

$$\mathrm{KE(iz)} = (1-\alpha_E)\mathrm{K}_{down}E(iz) \quad (22)$$

2.2.2.4.2. Longwave radiation

The surface temperature can be derived from the solution to the surface energy balance equation and requires air temperature T_a, wind speed v_{wind}, Bowen ratio B_0, storage heat flux Q_s, and net radiation flux Q as inputs. The surface temperature T_s is calculated as in Matzarakis et al. (2010) for each element (E(iz)). Bowen ratio is set as 20, a large value for assuming that latent

heat is negligibly small, and Q_s is calculated using OHM equations (Grimmond, Cleugh, & Oke, 1991). In that process, previous Q and present Q calculated with the previous surface temperature are used. When the model calculates the longwave radiation again, it uses the simulated surface temperature from Eq. (23):

$$\mathrm{T}_s = T_a + \frac{Q - Q_s}{(6.2 + 4.26 v_{wind})(1 + {}^{1}/_{B_0})} \quad (23)$$

The longwave radiation depends on view factors and emissivity. Like the net shortwave radiation, the net longwave radiation is the amount of downward (incident) longwave radiation $L_{down}E(iz)$ subtracted by the amount of upward (leaving) longwave radiation $L_{up}E(iz)$. $L_{down}E(iz)$ contains longwave radiation from the sky, as well as reflected and emitted longwave radiation from other elements. In the case of a building wall, the model follows Eq. (24):

$$\mathrm{L}_{down}B(iz) = \mathrm{F}_{sky \to B(iz)}\mathrm{L}_{sky} + \sum_{jz=1} F_{SB(jz) \to B(iz)} \left\{(1 - \varepsilon_B)LSB(jz) + \varepsilon_B \sigma \left(T_{SB(jz)}\right)^4\right\} + \sum_{jz=1} F_{R(jz) \to B(iz)} \left\{(1 - \varepsilon_R)LR(jz) + \varepsilon_R \sigma \left(T_{R(jz)}\right)^4\right\} + F_{G \to B(iz)}\{(1 - \varepsilon_G)LG(jz) + \varepsilon_G \sigma (T_G)^4\} + F_{W \to B(iz)}\{(1 - \varepsilon_W)LW(jz) + \varepsilon_W \sigma (T_W)^4\} + \sum_{jz=1} F_{V(jz) \to B(iz)} \left\{(1 - \varepsilon_V)LV(jz) + \varepsilon_V \sigma \left(T_{V(jz)}\right)^4\right\} \quad (24)$$

$L_{up}E(iz)$ is the reflected and emitted longwave radiation from E(iz) and depends on its emissivity by Eq. (25).

$$\mathrm{L}_{up}E(iz) = (1 - \varepsilon_E)LE(iz) + \varepsilon_E \sigma \left(T_{E(iz)}\right)^4 \quad (25)$$

2.2.2.4.3. Pedestrian MRT

MRT is calculated from the radiation from the urban elements surrounding a pedestrian. In this model, the urban elements include two walls (sunlit and shaded), two roofs (sunlit and shaded), two sidewalks (sunlit and shaded), a road, and the sky. These elements reflect direct and diffuse shortwave radiation and emit and reflect longwave radiation, which are summed using Eq. (26) from Matzarakis et al. (2010). The diffuse shortwave radiation is included in $K_{up}E(i)$.

$$\mathrm{MRT} = \left[\frac{1}{\sigma}\left\{\sum_{i=1}^{n} F_{i\to P}\left(LE_{up}(i) + \xi_k \frac{K_{up}E(i)}{\varepsilon_p}\right) + \xi_k \frac{K_{dir}P}{\varepsilon_p}\right\}\right]^{0.25} - 273.15 \qquad (26)$$

where ξ_K is the absorption coefficient, and ε_P is the emissivity of the pedestrian, which has standard values of 0.7 and 0.97 (Lindberg & Grimmond, 2011).

2.2.3. Model output tests

The study conducts three tests to evaluate the accuracy and application of the MMRT model: view factor evaluation, probability density profile evaluation, and a tree variable sensitivity test. For the latter two tests, this study selects the 244th day of the year (DOY, 1 September) in 2017 in an E–W street in Seoul (126.9658, 37.57142) as the tested area. 244 DOY was a

clear day without cloud and did not have rain back and forth. It also had high irradiance that led to lower thermal comfort. A street with an E–W orientation is used because N–S streets are mostly covered by building shade during the day and cannot show the difference between sunlit and shaded sides and the effect of the tree shade. The sensitivity test uses data from 1000–1600 LST, which is the period when a pedestrian experiences outdoor heat stress (Lee et al., 2013). Therefore, comparing MRT under sunlit and shaded areas is appropriate at this time. Table 1 shows the input data for the tests. This study selected 5, 1 m as the vertical layer thickness of building and tree, which can reflect vertical variance. Hence, these thickness is controlled by vertical variety of the study site.

Table 1. Input data for the model output tests.

Geometric data	Geometry	Street orientation (°)	Building height	Sidewalk width	Road width	Building vertical layer thickness Δz (m)	Tree vertical layer thickness Δzt (m)	Tree crown width cw (m)
	value	90	25	10	25	5	1	5
Meteorological data (1000–1600 LST)	LST	1000	1100	1200	1300	1400	1500	1600
	Air temperature (°C)	24	25.7	27.2	27.2	28.8	28.8	29.4
	Dew point temperature (°C)	11.6	11	10.8	11.6	11.8	13	12.7
	Cloud fraction	0						
	Wind speed	0.5						

	(m/s)	

2.2.3.1. View factor evaluation

A key part of the simulation new model is the calculation of the view factors using MCRT. This study validate these view factors using analytically calculated view factors for two cases that cover all the view factors in the model: adjacent lines at 90° and parallel lines (Fig. 6). This study adopted Howell's method for the analytic calculation (Howell, 1982). Orthogonal lines represent walls and sidewalks, whereas parallel lines represent areas between walls or the sky and sidewalk. First, the line length is set to 5 m. The height-to-width ratios are then changed from 0.2 to 6 in increments of 0.2. This study changes the number of rays (100, 1,000 and 10,000) to determine appropriate ray numbers for the model. These numbers are commonly used when verifying ray numbers (Z.-H. Wang, 2014).

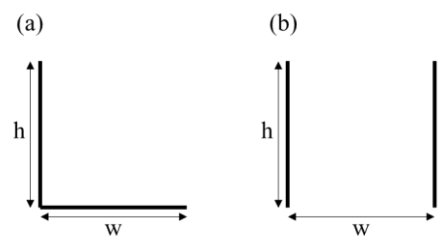

Fig. 6. Two orientations used for view factor validation: (a) orthogonal and (b) parallel.

2.2.3.2. Multi-layer variable evaluation

The advantage of the MMRT model is its ability to estimate MRT in an urban canyon with various building and tree probability density profiles. To the best of the authors' knowledge, only ENVI-met can accurately estimate MRT in the complex canyon with various building and tree heights (Lee et al., 2016). ENVI-met uses 3D input data to consider diversity. Meanwhile, the MMRT controls the probability density profile for vertical heterogeneity. This study evaluates these variables by controlling them in three cases (Fig. 7). For the building walls, case B1 is an urban canyon with 15 m buildings; case B2 is an urban canyon with 25 m buildings; and case B3 is an urban canyon with equal numbers of 15 m and 25 m buildings and without trees. For the trees, case T1 is 10 m tall trees; case T2 is 15 m tall trees; and case T3 has an equal number of 10 m and 15 m tall trees in one canyon. The building height in all three tree cases is 25 m. This study compares MRT between case 3 and the average of cases 1 and 2, which demonstrates the suitability of the density profiles.

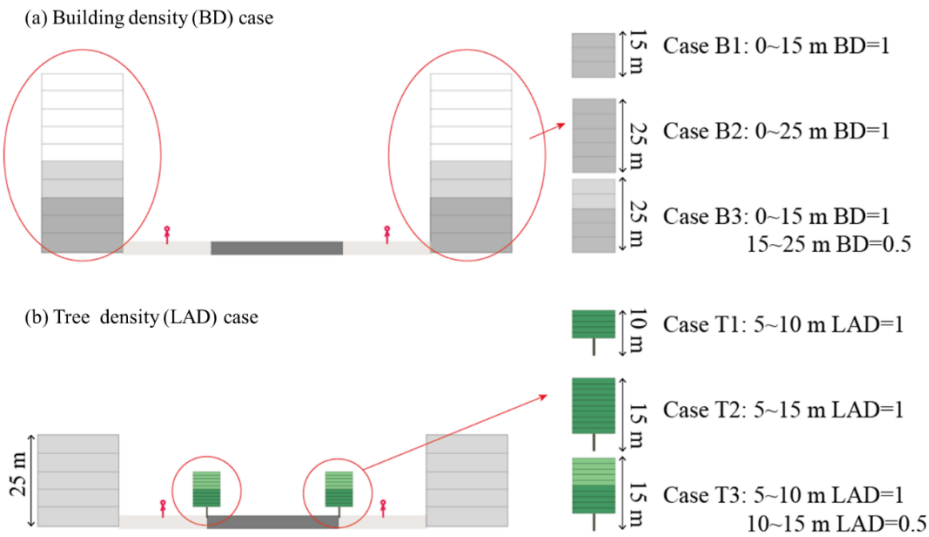

Fig. 7. Cases for the multilayer variation evaluation: (a) building cases B1–3 and (b) tree cases T1–3. The density (BD, LAD) varies depending on the case.

2.2.3.3. Tree variable sensitivity test

An MMRT model is good for manipulating tree parameters in addition to urban form and materials. For example, the shading effect of a tree is known as an effective MRT mitigation factor by reducing the shortwave radiation (Holst & Mayer, 2011; Kántor, Chen, et al., 2018; Konarska, Lindberg, Larsson, Thorsson, & Holmer, 2014; Lee et al., 2013, 2016). Therefore, the model's response must be checked by changing the main tree variables: tree height and LAD profile. This study can explore the effect of the tree planning strategies for the pedestrian radiation heat flux.

The LAD profile taken for the sensitivity test ranges from 0 to 1 with 0.25 intervals when the average tree height is 10 m. A tall street tree with 10 m

interval usually has 0.3 LAD. The average tree height is then changed from 6 m to 15 m (the tree crown starts at 5 m (Fig. 7)) in 1 m intervals. The LAD is fixed to 0.5 when the height is examined. Although the model assesses two sides of the pedestrians' MRT, this study focuses on the non-shaded side because it demonstrates the variation of MRT depending on the tree variables.

2.3. Results and discussions

2.3.1. Model output tests

Fig. A.1 shows the global radiation on 244 DOY, 2017. The modeled and measured global shortwave radiation showed difference. From 900 to 1500 LST, the measured radiation was greater than the modeled radiation. However, from 1500 to 2000 LST, the measured radiation was smaller than the modeled amount. The K modeling equations are from Allen et al. (1998) and developed in Italy. The error probably derives from the local difference. The environment surrounding the measured point affected the field data. In urban areas, buildings and obstacles create and influence shortwave radiation and lead to different model values (Gros, Bozonnet, & Inard, 2011). These findings should be further developed for accurate MRT results. However, the modeled and measured radiation trends closely resemble each other. The shortwave radiation reaches its maximum value at 1300 LST, then sharply drops after 1500 LST. In contrast, the global longwave radiation does not change much during the day because only small differences exist in air

temperature, which affects downwelling longwave radiation.

Total computing time is up to the sub functions: direct shortwave radiation and view factors. Computing time of view factors was 1062 s. Computing time of direct shortwave radiation varied with sun angle, and it ranged 10 to 16643 s. The total computing time of output tests (24 hours) was 45255 s. It can be reduced according to the ray movement method in the future.

2.3.1.1. View factor evaluation

As shown in Fig. 8, accuracy increased when the number of rays were increased. The simulation with 100 rays had a relatively larger RMSE (0.058 for the orthogonal lines and 0.050 for the parallel lines). Likewise, the results with 10,000 rays were fairly accurate compared to the analytical solutions with RMSEs of 0.005 (orthogonal lines) and 0.010 (parallel lines). In other words, 10,000 rays are sufficient to simulate accurate view factors in the model. Previous studies also confirmed that 10,000 rays result in negligible discrepancy (E. S. Krayenhoff et al., 2014; Z.-H. Wang, 2014).

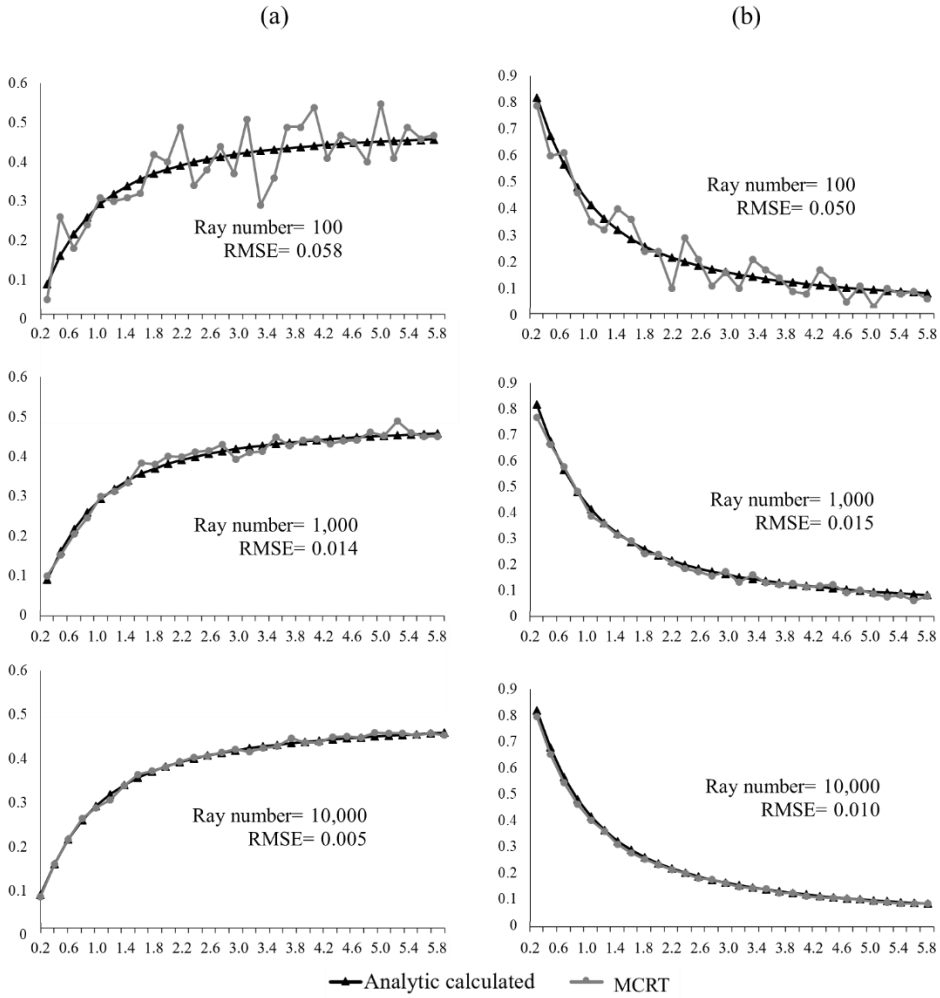

Fig. 8. Simulated (grey) and analytic (black) view factors. The left column shows adjacent lines at 90°. The right column shows two parallel lines. The X axis is the ratio of h and w.

2.3.1.2. Multi-layer variable evaluation

First, this study compared MRT results for varying buildings' probability density profile. In the building case (Fig. 9,) the average values of cases B1 and B2 and case B3 were similar, with a correlation R^2 of 0.9966 and 0.9968.

Hence, this study can estimate the pedestrians' MRT using the suggested multilayer model, especially for streets with diverse building heights. Some error occurred at 900–1500 LST in the sunlit area and from 1000 to –1400 LST in the shaded area. These errors came from the simulated shortwave radiation, especially for the building walls. The absorbed shortwave radiation by the shaded building walls tended to be overestimated in case 3, whereas the reverse was true for the sunlit walls.

For the tree case, the correlation coefficients between the average value of cases T1 and T2 and case T3 were statistically significant at 99.98% and 99.99%, respectively, showing that the tree LAD profile variable worked correctly.

Although this validation was limited to one scenario, the density profile can be divided in detail, making it possible to accurately represent the average radiation and MRT conditions along a street canyon with variable building heights with a single 2D geometry.

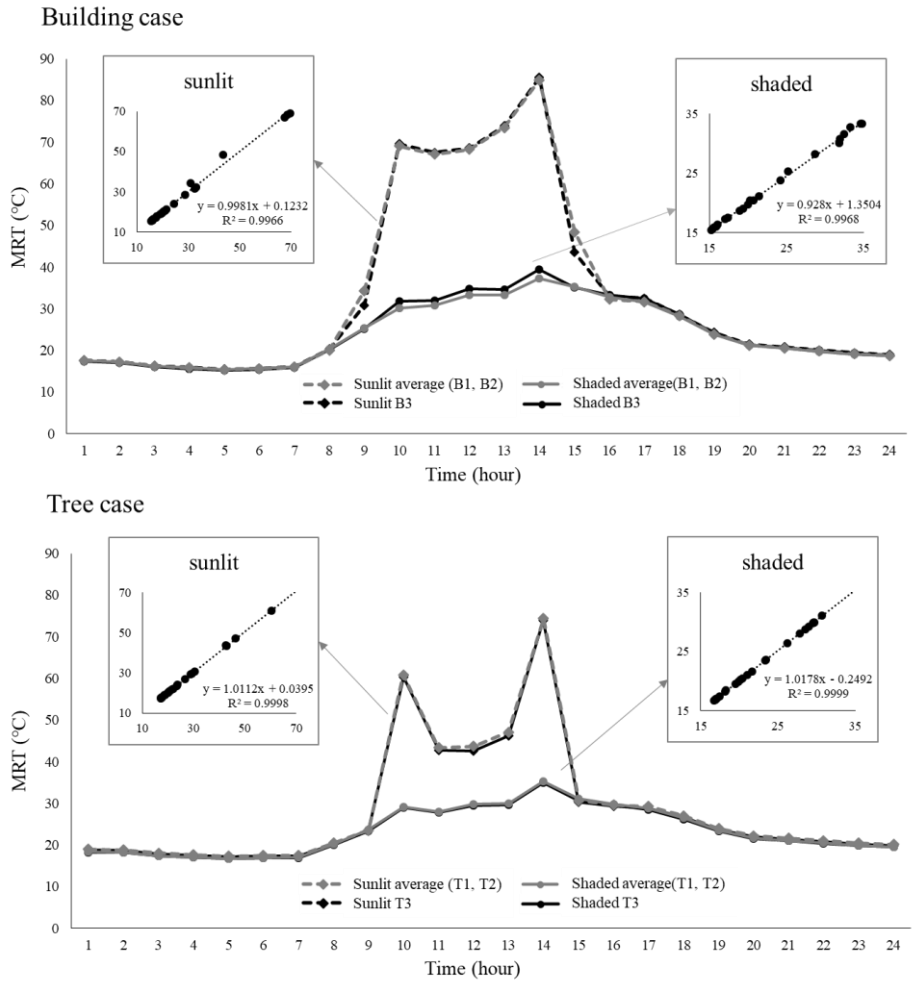

Fig. 9. Comparison of the average MRT in cases 1 and 2 and MRT in case 3. The X axis shows the mean time of day, while the Y axis denotes MRT. In the results in boxes, the X axis is MRT of case 3, while the Y axis denotes the average MRT of cases 1 and 2. The result of 1 September 2017.

2.3.2. Sensitivity test

MRT is calculated by summing up all the short and longwave radiation

flux densities from the 3D environment of pedestrians that are absorbed by them and greatly affected by the direct shortwave radiation. For this reason, this study compared two pedestrians on the sunlit and shaded (caused by buildings) sidewalks. During the 1000–1600 LST, only from 1000 to 1400 LST, the sunlit side pedestrian was completely out of the building shadow and MRT reduced by tree. On the other hand, the shaded side pedestrian was in the building shadow and had lower MRT. Both pedestrians were under the building shadow from 1400 LST.

This study then compared the results of the LAD scenarios. MRT on the sunlit side showed large decreases with the increasing LAD. The decrease of MRT caused by trees was largest in 1300 LST due to largest reduction in shortwave radiation. MRTs decreased by 2.7 °C (in shaded areas) and 23.1 °C (in sunlit areas) in 1300 LST (Fig. 10a) when the LAD increased from 0 to 1, which was very similar to the measured value from Kántor, Chen, et al. (2018). Fig. 10a shows that even if the profile density was large, a tree's shadow effect was less than that of the building shade, indicating that the shade on the sidewalks from the buildings and façades was crucial for reducing the pedestrians' MRT (Kántor, Gál, et al., 2018). The MRT reduction caused by trees was minor if the shadows from buildings already existed.

The MRT decrease was caused by the reductions of both shortwave and longwave radiations, although the reduction of the shortwave radiation was larger (Fig. 10b). At approximately 1300 LST on the sunlit side, the shortwave radiation decreased by 266 W/m². Almost all decreases were

caused by the reduction of the shortwave radiation from the sky, especially the direct solar radiation (Fig. 11a). The reduction from the sky increased when LAD increased, and was large in 1100–1300 LST. The reduction from the other elements was relatively small. The shortwave reduction from the sidewalk and the building wall was up to 15–20 W/m² (Figs. 10b and c). The reduction form wall was high in 1000 and 1600 LST when the shortwave radiation of the wall was low because of the tree shadow. The reflected shortwave from the sidewalk and walls also decreased, and the shortwave radiation reflected from the tree slightly increased. As for longwave radiation changes (Figs. 10d, e, and f), the amount coming from the sky and sidewalks decreased, but the longwave radiation from the trees offset these values increased.

The LAD profile can be controlled by tree species or spacing. For example, the street on which Zelkova serrata were planted at 10 m intervals had 0.3 LAD in the lower part and 0.15 in the upper part. MRTs could be lowered if the tree was changed to a denser-leaved species, or the spacing between the trees was reduced.

Previous research found that high LAD reduced shortwave radiation in an urban area. Takebayashi et al. (2014) found that trees reduced the shortwave radiation by 300 W/m² (50% of original) with a 6 m interval between trees. This effect was further lowered by more than 100 W/m² when the interval was 12 m. Similar with LAD, many previous studies emphasized the effect of LAI for reducing the shortwave radiation flux. A previous study found that

when the LAI increased from 2 to 6, the shortwave radiation reduction increased from 40 to 160 W/m², which was the maximum amount between 1200 and 1400 LST (Morakinyo & Lam, 2016; Ryu et al., 2016).

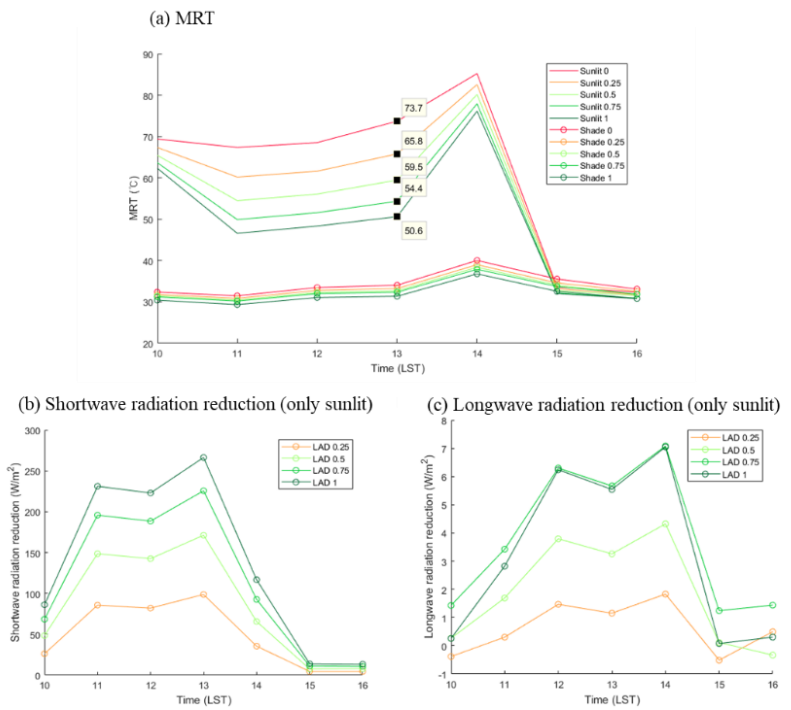

Fig. 10. MRT and radiation density changes by the LAD scenarios (0, 0.25, 0.5, 0.75, and 1). (a) MRTs under both sunlit and shaded area. (b) and (c) show the radiation reduction in the sunlit area. The result of 1 September 2017, 1000–1600 LST.

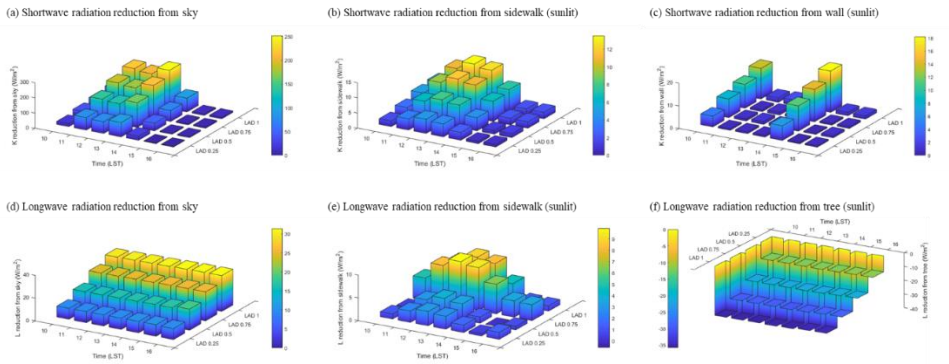

Fig. 11. Radiation reduction from the sky, sidewalk, and wall changed by the LAD scenarios (0.25, 0.5, 0.75, and 1) in the sunlit area. (a) Shortwave radiation reduction from the sky, (b) from the sidewalk, and (c) from the wall. (d) The result of 1 September 2017, 1000–1600 LST.

This study also conducted a sensitivity test for the tree height. The tree height scenario results were similar to the LAD scenario results: MRTs decreased as the tree height increased, and the decrease of MRT was the largest in 1300 LST. MRTs decreased by 3.6 °C (in the shade) and 19.2 °C (in the sunlit areas) in 1300 LST (Fig. 12a) when the tree height was 15 m. The taller the tree, the more MRT decreased. Note that MRT did not decrease much after 12 m because 12 m trees already fully shaded the pedestrian area and blocked the direct shortwave radiation from the sky (Figs. 11b and 12a). Thus, this height threshold can be varied by the sidewalk width or tree position.

This MRT reduction was caused by the shortwave radiation (Fig. 11b). At approximately 1300 LST, the reduced shortwave radiation from the sky reached 189 W/m², which was larger than the other elements' contributions

(sidewalks: 13.9 W/m²). The increased shortwave radiation reflected from the trees was negligible. As shown in Fig. 12c, the longwave radiation reduction gradually increased with the tree height increases. However, the amount of longwave radiation reduction was smaller than the shortwave reduction because of the emitted longwave from the trees (Fig. 13f). The reduced longwave radiation emitted from the walls was larger than the results of the LAD scenario, as indicated by the fact that taller trees can play an important role in preventing the longwave radiation from the ground. M. Wang, Chang, Merrick, & Amati (2016) asserted that tree height is an important factor because it showed a significant relation with the solar radiation reduction. Ryu et al. (2016) and E. S. Krayenhoff et al. (2014) also found that higher trees have great potential to mitigate urban heat by intercepting more radiation on the ground. However, note that taller trees can exert drag on the airflow in the urban canopy (E S Krayenhoff, Santiago, Martilli, Christen, & Oke, 2015), with potential implications for surface temperatures not included here for simplicity.

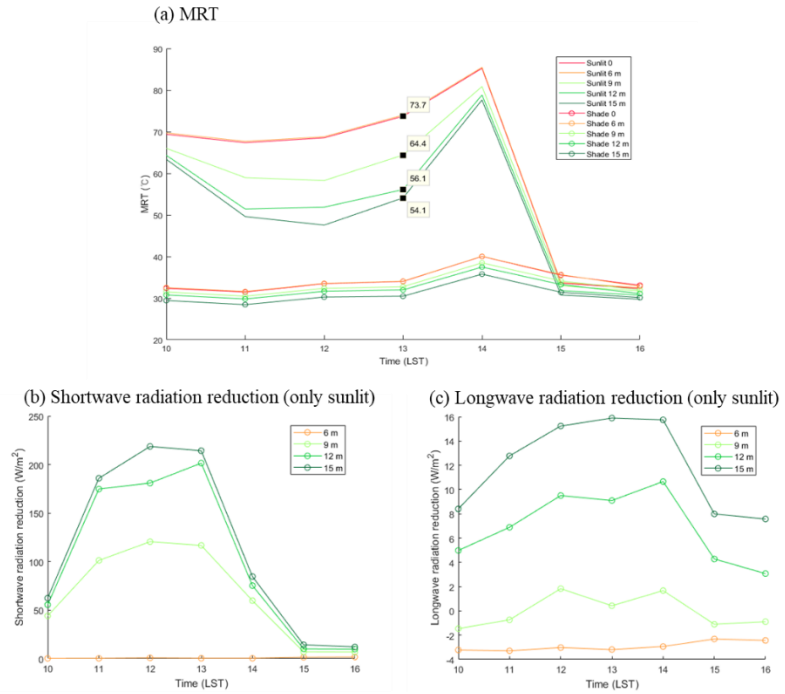

Fig. 12. MRT and radiation density changes by the tree height scenarios (0, 6, 9, 12, and 15 m). The cases in (a)–(c) are the same as those in Fig. 10.

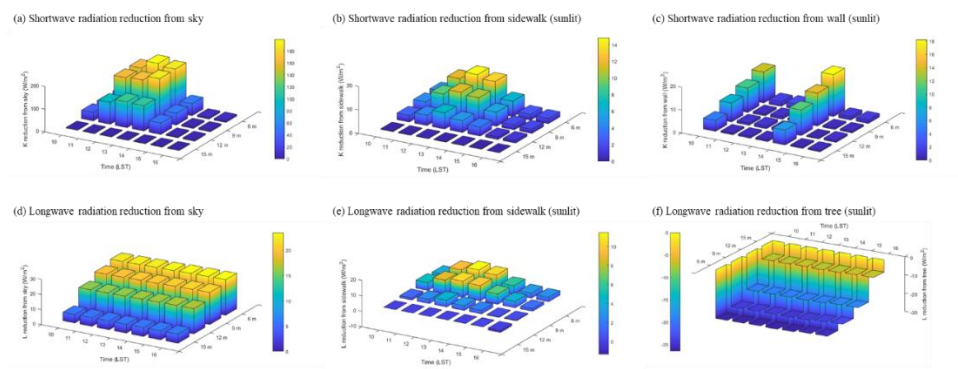

Fig. 13. Radiation reduction from the sky, sidewalk, and wall changed by the tree height scenarios (6, 9, 12, and 15 m) in the sunlit area. The cases in (a)–(f) are the same as those in Fig. 11.

This sensitivity test focused on 1000–1600 LST on 244 DOY with a specific urban form and pavement. These factors were very specific; hence, our results were difficult to generalize. However, our model showed skill in the estimation of the MRT variation with major factors affecting the pedestrians' radiation heat flux.

2.3.3. Model limitations and future development

An accurate estimation of the shading and surface temperature is the most important term in predicting MRT. Estimating the surface temperature relies primarily on shortwave radiation and reflection, which MMRT treats very accurately, and, secondarily, on the conductance of each of the energy dissipation mechanisms. Conductance relates to latent heat, sensible heat, and storage heat in the substrate. As regards the latent heat, the model used herein a very large Bowen ratio to make the latent heat very small. This needs an assumption for the model: the surface must have been dry at least for a day. In accurately calculating the sensible heat, the wind speed near the surface should be estimated. Some previous research estimated the wind speed using complex approaches, such as 1D turbulent diffusion models (E S Krayenhoff et al., 2015) or CFD approaches (Bruse & Fleer, 1998). However, this study aim to build a new model that reasonably estimates MRT without this computational expense. Therefore, this study assumed that the wind speed at the pedestrian level was constant. Nevertheless, the MMRT represents

radiation transfer, particularly with respect to its attenuation by trees, with an equal or higher fidelity approach than taken in other models, including a CFD. Finally, the storage heat was calculated using OHM equations; however, it could be represented in a more physical manner by including a multi-layer conduction model, which would be part of the future work. This study considers the three final conductance: modifications that could be made to the surface energy balance equation to more physically represent other heat dissipation mechanisms, as secondary to the estimation of MRT of a pedestrian, provided they are reasonably well represented.

The model used a constant value of air temperature, dew point temperature, and wind speed within a street canyon, which can lead to an incorrect result for higher values of H/W. However, these assumptions are made in most urban canopy models, for example, in RayMan and SOLWEIG models. ENVI-met presents the only model that claims to represent the spatial variation of these terms within the canopy in 3D, but it requires extensive computational resources and setup time, and has limitations with respect to its representation of trees, which is the core objective of the current work. Therefore, the current version of the MMRT is likely to be less reliable for higher H/W values. This limitation can be developed in the future work.

2.4. Conclusion

This study proposed an MMRT model for estimating MRT of pedestrians

in a street canyon. The advantage of the model is that it simulates radiation transfer in a complex urban street with equal road width and randomly ordered building height using simple input data. This model uses the MCRT method for view factor determination and includes the probability density profile to consider the vertical heterogeneity of urban areas. This study also verified the effectiveness of these methods. The MCRT evaluation showed little RMSE (0.005, 0.01) with 10,000 rays per model element. This number provided sufficient model accuracy. This study also evaluated the probabilistic density profile variable to representing buildings and tree leaves by comparing it to the average of its constituent (non-probabilistic) density profiles. Our results indicated that the probabilistic approach was suitable.

The MMRT model was optimized to calculate the pedestrian MRT and inform street design. The shading effects of trees can be assessed using this model. This study conducted a sensitivity analysis by modulating the LAD and the tree height, and for a particular summer scenario considered, the model indicated that MRT of a pedestrian in the sunlit area can be reduced by approximately 23 °C in 1300 LST. The LAD increased to 1 m2 m−3 from 0 m2 m−3 and 18 °C as the tree height increased from 6 m to 12 m in 1300 LST mainly because it reduced the solar radiation from the sky. The study calculated the effects on MRT not only from the tree variation, but also from the changes to urban form and pavement.

Although the MMRT model has many advantages, it is still in development and can be further improved. Estimating the surface temperature

can develop a more complex and accurate method. Model evaluation with field measurement and simulated results should be performed in addition to the model verification performed. These results provided helpful guidelines for designing thermal-friendly streets based on urban form, pavement, and trees.

Acknowledgment

This work was supported by the Korea Agency for Infrastructure Technology Advancement (KAIA) [grant number 18AUDP-B102560-04] and by the BK 21 Plus Project in 2017 (Seoul National University Interdisciplinary Program in Landscape Architecture, Global Leadership Program toward innovative green infrastructure).

III. CHAPTER 2: Variations in pedestrian mean radiant temperature based on the spacing and size of street trees

3.1. Introduction

Urban areas are projected to warm as a result of climate change and urban development (Scott Krayenhoff & Voogt, 2016; Stewart & Oke, 2012). In this context, it is increasingly important that urban areas be designed to offset high summertime temperatures. Increased built surfaces at the expense of vegetated surfaces modifies the radiation balance and increases sensible heat flux, which cause a negative effect on people, including: discomfort, lower productivity, and heat-related diseases (Brown et al., 2015; J. Wang et al., 2015). Some street canyons contain pedestrians who are particularly vulnerable to increased urban heating. Most streets are made of impervious surfaces and little vegetation. Also, cars and buildings are anthropogenic heat sources. Consequently, urban planners are considering heat mitigation strategies to prevent further increases in urban heating on streets. Critically, pedestrian thermal exposure depends on several factors in addition to air temperature, in particular the radiant environment in urban street canyons.

Many heat mitigation strategies are used in existing urban areas, including converting impervious surfaces to cool or permeable surfaces, providing water bodies, increasing the amount of vegetation, and green infrastructure

(Dimoudi et al., 2014; L. Kong et al., 2017; Lee & Mayer, 2018b; Rizwan et al., 2008; Rosso et al., 2018; Takebayashi et al., 2014; Tominaga et al., 2015; Zoras et al., 2014). Increasing the amount of vegetation, particularly trees, is a well-known strategy to effectively reduce urban heat (Lee & Mayer, 2018a; Lee et al., 2016; Zölch, Maderspacher, Wamsler, & Pauleit, 2016). Increasing vegetated area helps address a root cause of urban warming (Norton et al., 2015). In addition, it can provide diverse ecosystem services, such regulating stormwater and absorbing carbon, which make cities more resilient to climate change (Foudi, Spadaro, Chiabai, Polanco-Martínez, & Neumann, 2017; Maria Raquel, Montalto, & Palmer, 2016). For these reasons, urban planners often opt to plant trees as a heat mitigation strategy (Z. Wu & Chen, 2017).

Planting trees mitigates urban heat by two methods: providing a shading effect and converting solar radiation to latent heat flux through transpiration (Konarska et al., 2016; Rahman, Moser, Rötzer, & Pauleit, 2017; Zölch et al., 2016). Trees directly reduce the incident radiation on surrounding surfaces by shading (M. Wang et al., 2016). And trees intercept sunlight energy and use it for transpiration, which cool leaves and the surrounding air compared to built surfaces especially at midday (David Armson, Rahman, & Ennos, 2013). Although both effects are important for reducing urban heat, the shading effect represents the majority (80-95%) of the air temperature cooling at the micro scale (L. Shashua-bar & Hoffman, 2000; Zardo, Geneletti, Pérez-soba, & Eupen, 2017).

The cooling effect of trees, especially their shading effect, has been

recently investigated during the last decade. Tree shade reduced solar radiation up to 76~93 % during summer (Abreu-Harbich et al., 2015; Holst & Mayer, 2011).This radiation reduction improved thermal comfort. During the day, reduced radiation flux resulted in physiologically equivalent temperature (PET) reduction from 0.84 to 17.5 K (varies depending on species) during the day (Abreu-Harbich et al., 2015).

Even though many previous studies have reported the cooling effect of trees, they have not provided specific design parameters that can be applied to urban planning. Some studies have measured the reduction of urban heat due to trees at specific field study sites (D. Armson, Stringer, & Ennos, 2012; Klemm, Heusinkveld, Lenzholzer, & van Hove, 2015; Lee et al., 2013). However, these results are limited to the study site and are difficult to apply to other areas. Other studies have used numerical simulations to confirm that larger and denser trees are more effective at intercepting radiation, reducing sensible heat flux, or mitigating urban heat (E. S. Krayenhoff et al., 2014; Morakinyo & Lam, 2016; Ryu et al., 2016). Solar radiation interception (and therefore effective heat mitigation) of trees typically increases as the leaf area index increases (E. S. Krayenhoff et al., 2014; Morakinyo & Lam, 2016; Ryu et al., 2016) and as tree height increases (E. S. Krayenhoff et al., 2014; Ryu et al., 2016). These results are also difficult to apply to urban planning because the urban planner must select trees within limited space and budget, which are relatively fixed parameters. However, when provided with a range of options and evidence for optimal tree size and tree tree spacing, planners

have more relevant information in terms of tree-planting decisions.

Moreover, applying the results of previous studies to urban planning is also difficult because most studies report the cooling effect of trees for limited times or days. They suggest that their results can represent the hottest days of the year (Lee & Mayer, 2018a; Lee et al., 2016; Lee, Mayer, & Kuttler, 2018; Taleghani, Tenpierik, Dobbelsteen, & Sailor, 2014; Zölch et al., 2016). However, such days occur only a few times a year, which makes planning based on these infrequent conditions risky. Research should evaluate the cooling effect of trees over the entire summer period.

The purpose of this study is to determine how effectively trees reduce pedestrian exposure to radiation during the summer, depending on the spacing between trees and size. The mean radiant temperature (MRT) is used as the metric for assessment of the thermal impact of trees. MRT is one of the most important variables for assessing thermal comfort, and integrates exposure to shortwave and longwave radiation in a three-dimensional environment (Holst & Mayer, 2011; Lee et al., 2013; Thorsson et al., 2007). To reflect the total period during which heat stress could be a problem (Holst & Mayer, 2011; Lee & Mayer, 2018a, 2018b; Lee et al., 2016), this study uses the average reduction in MRT during the period 10:00–16:00 LST from June to August (for days with a cloud fraction of less than 50%). MRT was simulated by changing the tree spacing incrementally. Four types of trees and two street types were used to evaluate various tree and street sizes. The main research questions of this study are as follows:

1) How does the reduction in pedestrian MRT due to street trees vary depending on the spacing between trees?

2) How does the reduction in pedestrian MRT due to street trees differ depending on the tree size?

The hypothesis testing was done with two types of streets. The results of this study fill the gap between the researches on the cooling effect of trees. It can provide the insight into optimal configurations of street trees. It will help urban planning mitigate radiation exposure by providing data on both spacing, size and their radiation absorption processes.

3.2. Methods

3.2.1. Research flow

This study is simulation-based, with the MMRT model used to assess pedestrian MRT. The average reduction in MRT, given variations in spacing between trees and sizes, is calculated; nine scenarios are investigated by changing the tree and street sizes (No trees + 4 tree sizes × 2 street sizes) and this study changes the spacing between trees in each scenario (Fig. 14). From MRT reduction results, this study discusses the appropriate tree spacing and size. Also this study mentions the reasons for variations in MRT due to tree size by examining the reduction in incident radiation on the pedestrian from the urban elements.

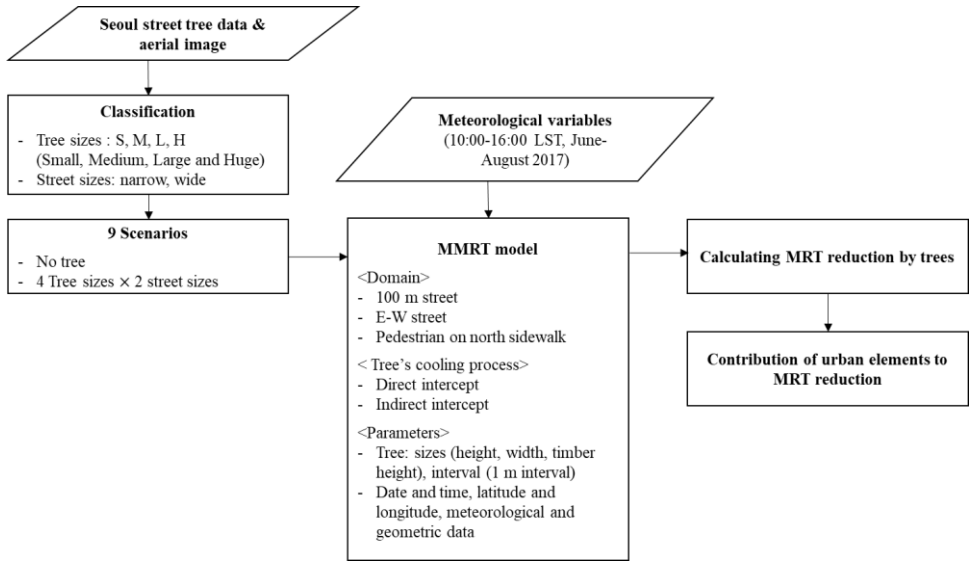

Fig. 14. Flowchart of the study.

3.2.2. MMRT model

3.2.1.1. Model domain and assumptions

This study aims to determine the variations in MRT due to trees in a street canyon. The study site is a 100 m street on one block. In the MMRT model, the 3D street canyon is compressed into a 2D based on the following assumptions. (1) The size, spacing, and planting location of the trees are uniform throughout the block. (2) There is no anthropogenic heat flux, and; the model considers only shortwave and longwave radiation from urban elements, including the sky, and their reflections. Estimating anthropogenic heat flux in a micro scale is difficult because of its variation. Moreover anthropogenic heat flux differs from, and is unlikely to substantially affect, radiation flux (Järvi, Grimmond, & Christen, 2011); (3) pedestrians

(represented as a 2 m line) walk in the center of the sidewalk; (4) the street is oriented E–W (90 degrees), pedestrians walk center on the S-facing street (the N-facing sidewalk of the street is in the shadow of the buildings, thus there is little shading effect from the trees).

3.2.1.2. Fundamentals of the MMRT model

The MMRT model developed based on a multi-layer urban canopy model geometry and the calculation method is derived from Krayenhoff et al. (2014), Allen et al. (1998), and Matzarakis et al. (2010). After calculating view factors, solar radiation and longwave radiation from each element and radiation received by the pedestrian are calculated at each hour. This study aims to reveal the variation of shading effect using the MMRT model. Before applying the MMRT model, this study validated this model with measured MRT (Appendix B).

3.2.1.3. Cooling effect of trees

Trees reduce pedestrian exposure to radiation in two ways. Trees reduce radiation incident on pedestrians from sky and urban elements (i.e. buildings, roads, and artifacts). Also trees shade nearby surfaces; as a result, the surface temperature of the latter decrease, as does the amount of longwave radiation that the pedestrian is exposed to. The shading effect plays a key role in

reducing the MRT of pedestrians in a street. In the model, MRT is calculated using Eq. (26)

Where the E(i) are the urban elements, including building walls, roofs, sidewalks, roads, trees, and the sky; and the $F_{E(i)\rightarrow P}$ are the area-weighted view factors from E to the pedestrian, P. $L_{up}E$ and $K_{up}E$ are incident longwave and shortwave radiation from E, and $K_{dir}P$ is the incident direct shortwave radiation from the sky (W/m2). ξ_k is the absorption coefficient (0.7) and ε_p is the emissivity of the pedestrian (0.97).

Before calculating the MRT, shortwave and longwave radiation leaving each element must be calculated. To evaluate longwave emission, surface temperature is calculated based on assumed surface Bowen ratio and calculated storage heat flux (Matzarakis et al., 2010). The storage heat flux is determined using the OHM model (Grimmond & Oke, 2002).

Trees intercept radiation differently compared to solid objects in the urban environment. They prevent incident shortwave and longwave radiation arising from other urban elements (walls, sidewalks, road, and the sky) from reaching pedestrians and nearby surfaces. As incident radiation reaches the tree canopy, a certain amount of it is blocked until the radiation passes out. The ratio of intercepted energy is expressed by Eq. (27).

$$\text{Tree intercepted fraction} = 1 - \exp\left(-K_{bs}\Omega LAD\frac{w}{x}\right) \qquad (27)$$

Where K_{bs} is the extinction coefficient of the leaves and Ω is the clumping factor. The clumping factor ranges from 0 (clumping leaves) to 1

(random distribution) to generate differences in the probability of radiation being intercepted (Q. Chen, Baldocchi, Gong, & Dawson, 2008; E. S. Krayenhoff et al., 2014). As the aim of this study is to determine the shading effect of trees depending on the spacing between trees, the average density of the tree canopy in a (100 m) street is assessed according to the space between trees (= w/x) (Fig. 15). The tree canopy is simplified as a box, and the leaf area density (LAD, m2/m3) and clumping factor of each tree layer are defined as having values of 1. Assuming a spherical leaf angle distribution, the extinction coefficient is set at 0.5 (E. S. Krayenhoff et al., 2014).

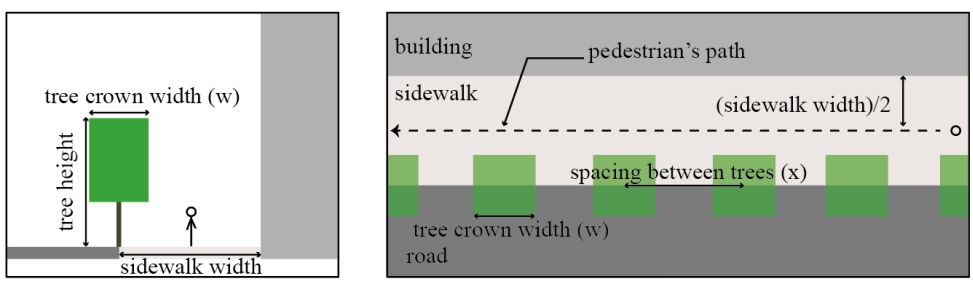

Fig. 15. Tree input variables for the model (left: side view, right: top view).

The process of interception reduces MRT of the pedestrians. However, trees can also increase the exposure of incident radiation to the pedestrian by emitting longwave radiation (Fig. 16).

$$\text{Longwave radiation emitted from trees} = (1-\varepsilon_T)LTree + \varepsilon_T\sigma(T_{Tree})^4 \ \text{(W/m2)} \quad (28)$$

This process is modeled using Eq. (3). ε_T is emissivity of trees and σ is Stefan-Boltzman constant (5.67x10-8 Wm-2K-4). $LTree$ and T_{Tree} is the incident longwave radiation to the tree and tree surface temperature (W/m2). Some of the incident radiation striking the tree is reflected to the area surrounding it (Fig. 16). Depending on the direction in which it is reflected, it can either lower MRT or increase it. More information on radiation transfer methods employed in the model can be found in E. S. Krayenhoff et al. (2014) and Park et al. (2018).

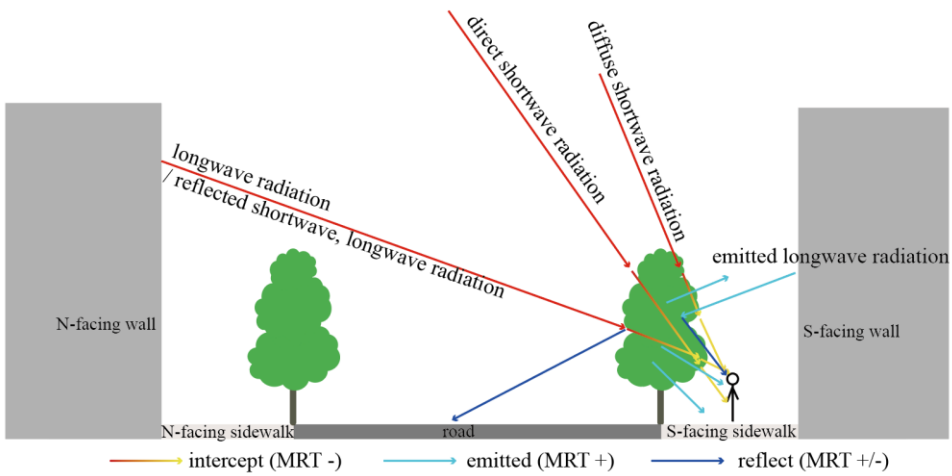

Fig. 16. Radiation processes of a tree and their effect on MRT in the street canyon.

3.2.3. Model parameters

3.2.3.1. Simulating scenarios

The purpose of this study is to determine how the reduction in MRT varies depending on the spacing between trees. However, the former is also affected by tree size. Four classes of tree size were identified using tree data on the streets of Seoul (data.seoul.go.kr). The tree height and canopy width were averaged within each class. Actual street sizes (road width, sidewalk width, and building height) are very diverse and difficult to classify. Two street types were selected to represent medium- and large-sized streets, assigned as widths of 15 and 30 m, respectively, in the model. The general width of the sidewalk and heights of the buildings corresponding to the two streetscapes were defined using aerial images of Seoul.

MRT was simulated eight times using these tree and street canyon types. In each simulation, the spacing between trees is increased 1 m from the minimum value (= w). As the MMRT model uses a 2D domain compressed from a 3D environment, the spacing between trees (x) is considered in the percentage of tree canopy (w/x).

3.2.3.2. Input variables

The input data for the MMRT model were classified into 4 categories: date and time, latitude and longitude, meteorological data, and geometric data. The date and time data was related to the study temporal range: 10:00–16:00 LST on clear days (cloud fraction under 50%) during June–August, 2017. The number of days satisfying the condition was 21 (Table 2). Each change in the

date and time results in a change in the solar angle. Using data from the Korea Meteorological Administration, clear days were selected, and corresponding air temperature and dew point temperature were used for the meteorological data input (Table 2).

Table 2. Meteorological data for the MMRT simulation (10:00–16:00 LST, June–August, 2017).

Date (DOY)	Cloud fraction (0-100 %)	Air temperature (℃)							Dew point temperature (℃)						
		10	11	12	13	14	15	16	10	11	12	13	14	15	16
153	22.5	21.3	22.8	23.6	24.3	25.3	25.4	24	2	0.5	3.4	1.8	2	3.3	6.7
154	22.5	21.3	22.3	24	24.6	25.1	26.2	26.4	8.2	6.4	5.8	4.8	4.7	5.7	6.4
155	17.5	23.7	25.1	26.4	26.8	27.3	27.8	27.8	3.5	3.6	3.5	3.2	3	5.3	5.3
159	27.5	20.4	22	23.3	24.7	25.5	25.5	24.6	13.8	14.6	13.7	13.2	10.8	12.6	13.1
162	1.3	24.3	26	27.2	28	28	28.4	29.2	5.6	4.9	5.4	3.6	2.2	2.5	5.2
165	25	22.5	23.7	24.6	25.9	26.6	26.8	26.7	12.7	14.1	13.4	13	12.6	12.8	11.9
166	6.3	22.7	24.5	26.6	28.6	29	29.4	28.8	15	14.5	13.6	13.6	11.9	12.7	12.6
167	0	26	27.6	29.2	30.3	32.1	32.6	31.7	16.2	14.9	13.8	14.3	14.2	13.7	16.4
168	0	25.1	26.6	27.9	28.4	28.5	29.2	29.6	13.9	13.3	13.7	14.6	12.7	11.2	10.6
169	1.3	25.8	27.2	28.8	30.1	31.1	31.5	30.4	12.2	10.3	10.4	10.1	10.4	11.3	12.3
172	27.5	27.5	27.8	29.6	30.8	31.5	30.6	30	13.4	11.7	11.1	12.1	12.8	12.4	11.9
173	47.5	25.8	27.8	28.5	29.8	30	30.1	29.6	16.3	15.1	13.9	15.5	17.4	16.5	16
174	32.5	28.5	30.1	30.6	32.7	33.8	33	32.9	15.7	15	15.4	11.8	12.1	16.3	17.8

181	42.5	27.1	28.4	29.1	29.9	30.2	30.7	30.3	18.1	18.4	19.1	18.3	17.2	17.3	18
186	50	26.9	28.6	30.3	31.3	31.6	31.3	32	20	19.2	20.2	19.3	19.5	18.6	19.2
201	31.3	29.7	31.1	32	32.4	33.9	34.9	34.6	22.1	22.9	22.1	23.3	22	22.2	22.9
206	41.3	29.7	30.9	32	33	33.6	34.4	34.9	21.6	21.6	21.5	20.8	20.3	21.1	20.4
207	23.8	28.8	29.8	31	31.3	32.3	32.6	32.7	18.2	17.6	17.6	18.6	19.1	20.1	18.8
219	37.5	29.3	30.4	32.1	33	33.5	34	34	22.2	22.2	20.3	21.8	19.9	23	18.8
238	8.8	24.7	26.2	27.2	28	28.7	28.8	28.9	6.8	7.2	10.8	8.2	7.8	8.9	8.5

The latitude and longitude were the location of the Seoul weather station for the Meteorological Administration: 37.57° N, 126.97° E. Lastly, the geometric data were determined by the defined tree and street sizes.

3.2.4. Calculating MRT reduction due to trees

To assess MRT reduction due to trees, MRT values in the scenarios with trees were compared to the ‘No tree’ scenario, which had all the same input data except for the tree variables. As the number of clear days (cloud fraction of less than 50%) during the summer is 20, a total of 140 simulations (7 h for each of 20 days) were conducted. Finally, this study calculates the average amount of MRT reduction for a certain type by taking the mean over 140 times.

3.3. Results and discussions

3.3.1. Simulating scenarios

3.3.1.1. Tree and street sizes

Trees planted in Seoul have very diverse sizes. In this study, they were divided into 4 classes (S, M, L, and H) based on tree height using the natural breaks classification method. The tree height and tree width within each class were then averaged. Detailed information regarding the four tree classes is provided in Fig. 17. As this data is based on the current situation, most of the trees in each class were planted years ago and have undergone management such as trimming, but some were newly planted. This means that urban planners should apply the results of this study carefully when planning to plant new trees. They may need to consider the grown or managed size of tree.

3.3.1.2. Street types

The streets in the city are divided into two sizes based on the road width: narrow roads with a width of 15 m, and wide roads with a width of 30 m. The sidewalk width and building height were defined as 5 m and 15 m for the narrow street (h/w: 0.6), and 7 m and 25 m for the wide street (h/w: 0.57), respectively.

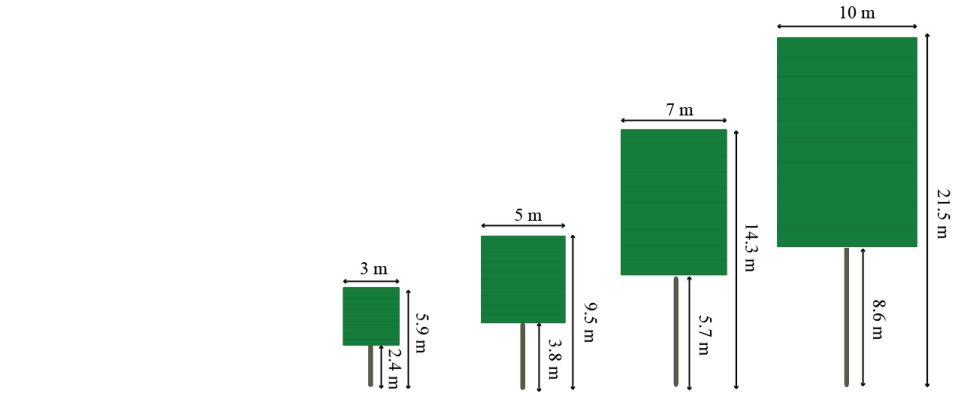

Types	S	M	L	H
tree height (m)	5.9	9.5	14.3	21.5
clear-bole length (m)*	2.4	3.8	5.7	8.6
tree crown width (m)	3	5	7	10

* clear-bole length = tree height x 0.4

Fig. 17. Parameters of the four tree classes.

3.3.2. MRT reduction

3.3.2.1. Average MRT reduction

The average MRT reduction from the total study temporal range (10:00–16:00 LST, June–August) was determined for all scenarios (Fig. 18). When the trees are planted without spacing, MRT decreases by approximately 20.7–33.7 K, which varies with tree size. For a tree spacing of 11 m on the wide street, the average MRT reductions are 9.5, 20, 22.1, and 33.1 K on average for tree types S, M, L, and H, respectively. Those amounts represent 19–67 % of 'No tree' scenario (the average MRT is 322.9 K). These results demonstrate the importance of trees for reducing MRT of pedestrians. These results vary with the street size. For instance, type H trees reduce MRT by 23.5 K more than S type trees, which suggests that smaller trees need to be

planted at closer spacing to reduce the same amount of MRT. The reason for this difference between tree sizes is explained in the following section.

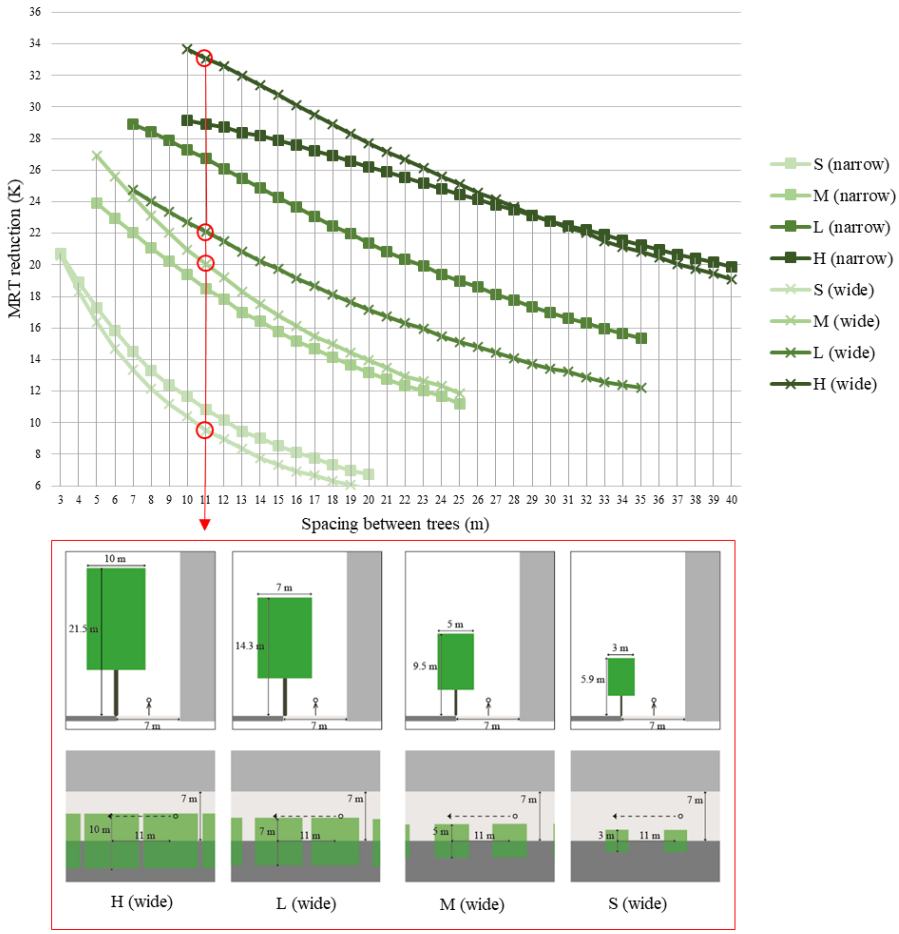

Fig. 18. MRT reduction depending on spacing between trees, tree size, and street size; the line color corresponds to the tree size (S, M, L, and H), square dots correspond to the narrow street and x-shaped points correspond to the wide street. The lower figure depicts the location of street trees for a tree spacing of 11 m (wide street).

Regardless of the tree size and the street size, MRT reduction increases as the tree spacing decreases (Fig. 18). Takebayashi et al. (2014) also reported

that a narrower tree spacing could absorb more radiation. However, their model only simulated four different spacing (6, 8, 10, and 12 m), which limits its ability to explain the form of MRT reduction depending on tree spacing. In this study, the reduction slope was calculated by subtracting MRT reduction value for one tree spacing from that of the following spacing (i.e., the slope of the graph in Fig. 18). As shown in Fig. 19, the reduction slope tends to increase as the spacing decreases for S and M size trees, indicating that MRT reduction effect increases exponentially as the tree interval becomes narrower. For the S type trees, the slope appears to increase dramatically from the spacing of 10 m (1.7 for 3-7 m, 0.9 for 8-10 m). This indicates that narrowing tree spacing of the range of 3-10 m is more effective for reducing MRT than doing for the range of above 10 m range. As a result, it is suggested to plant S size trees with an interval of at most 10 m, and the smaller the spacing, the better. This change comes from the variation of intercepted direct solar radiation by trees. However, in the case of M and H size trees, the slopes don't increase as the spacing decrease. The result came from the initial shading of direct solar radiation. In the case of large trees, even though they are spaced at wide spacing, they can block lots of amount of direct solar radiation. Therefore, narrowing the tree spacing doesn't significantly increase MRT reduction compared with smaller trees. As the tree size increases, MRT reduction slope does not vary substantially with the spacing between trees. Because decreasing the interval has a similar effect at any interval, a planner can choose the preferred tree spacing by taking into account various other variables such as cost.

The benefit of high tree density in a street canyon also appears in the transpiration cooling effect as well as shading effect (Rahman, Moser, Gold, Rötzer, & Pauleit, 2018). For this reason, when urban planners select a smaller tree spacing or larger trees, both the shading effect and the transpiration effect would increase and the total thermal benefit may be larger than this study calculates in this study.

In this study, the analysis was based on fully-grown trees. However, tree growth must be considered in any street planning exercise. When a planner plants young trees, they should set the spacing between trees to account for the potential for MRT reduction of fully-grown trees. Even smaller trees with sufficiently narrow spacing will have larger effects in the future.

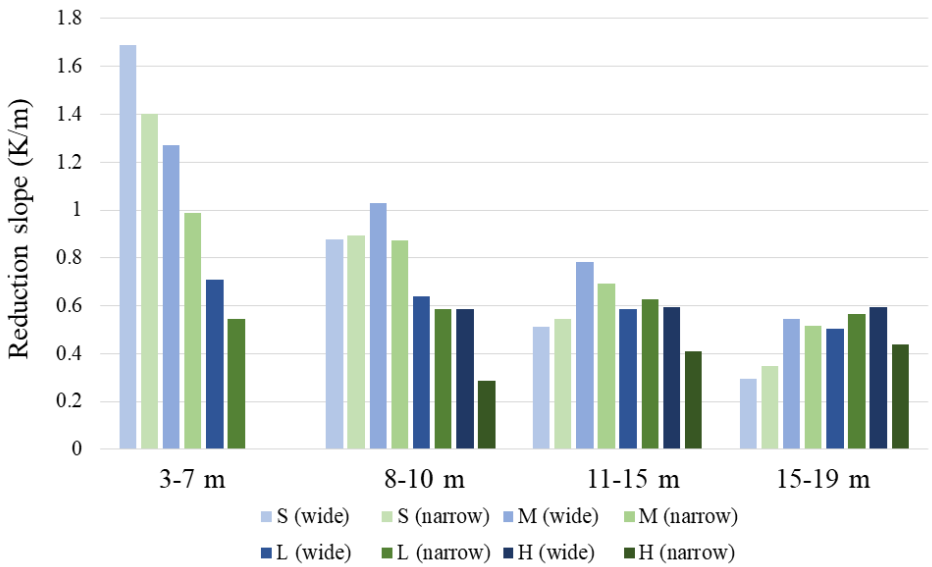

Fig. 19. Average MRT reduction slope (K/m) for a certain ranges (3-7 m, 8-10 m, 11-15 m, and 15-19 m). X-axis means the range of spacing between trees.

Notably, there is no substantial difference between narrow and wide streets for the E–W street (Fig. 18). First, it shows that the trees are more important than the street geometry for reducing MRT of pedestrians on the S-facing street. In other words, shade has the most significant impact on MRT (Holst & Mayer, 2011; Mayer et al., 2008). In the same vein, shade from the buildings is the most important factor for pedestrians on the N-facing street. As the incident shortwave radiation plays a significant role in increasing the amount of radiation exposure, blocking direct shortwave radiation with a canopy can be the effective strategies for reducing heat (Lee et al., 2013). Second, the two street sizes have a similar sky view factor (SVF). There is a clear relationship between the SVF and urban thermal comfort during the daytime (Ali-Toudert & Mayer, 2006; Coutts, White, Tapper, Beringer, & Livesley, 2016; Lee et al., 2014). Pedestrians in a street canyon with a large SVF are vulnerable to radiation exposure because of the high amount of incident radiation from the sky.

3.3.2.2. Radiation contribution of urban elements to MRT reduction

As previously mentioned, reducing the amount of incident radiation from the sky with tree canopies is important for MRT reduction. To confirm this, the reduction in the radiation incident on pedestrians due to urban elements was calculated. The radiation reduction was averaged for tree spacing ranging

from the minimum to +17 (the n for averaging is 18). Urban elements include the sky, walls (S and N-facing), S-facing sidewalk, and road. The contribution of the N-facing sidewalk and roof were ignored for MRT. As expected, the radiation reduction from the sky accounts for 64–75% of the total reduction and it appears largest in small trees (Fig. 20). In addition, the reduction in shortwave radiation was larger than the reduction in longwave radiation and the amount of reduction increases as tree size increases (Fig. 21). The reduction in shortwave radiation mainly resulted from the trees intercepting direct shortwave radiation. Trees can provide shades to pedestrians and reduce the SVF to reduce their exposure to solar radiation. The effect of providing shade and the SVF reduction effect increases up to the H size.

The next largest reduction in radiation due to the trees is that in the radiation reflected off the S-facing wall and sidewalk (Fig. 20). This reduction also increases as the tree size increases because of increasing the amount of intercepted shortwave and longwave radiation. When trees are planted on the street, they intercept the incident shortwave radiation to the S-facing wall and sidewalk. This decreases the reflected shortwave radiation from the wall and sidewalk. Furthermore, this interception can reduce surface temperature on the nearby surfaces, thus reducing the emitted longwave radiation from the surfaces. The reason why the longwave reduction is greater in the sidewalk than in the wall is because the surface temperature of wall is higher.

The other elements are the N-facing wall and road, which are located outside of the trees from the perspective of the pedestrians. Because of their

position, trees can directly intercept radiation from the N-facing wall and the road, especially the emitted longwave radiation. As shown in Fig. 21, the amount of shortwave radiation is small, which means that already shaded areas have a smaller contribution to MRT than sunlit areas. From the N-facing wall, the longwave reduction increases with trees up to L size (with a height of 14.3 m and timber height of 5.7 m), then decreases.

From the results for the walls (S and N facing), sidewalk, and road, it can be concluded that although the processes of intercepting shortwave and longwave radiation from the urban elements are different, the reduction increases as tree size increases.

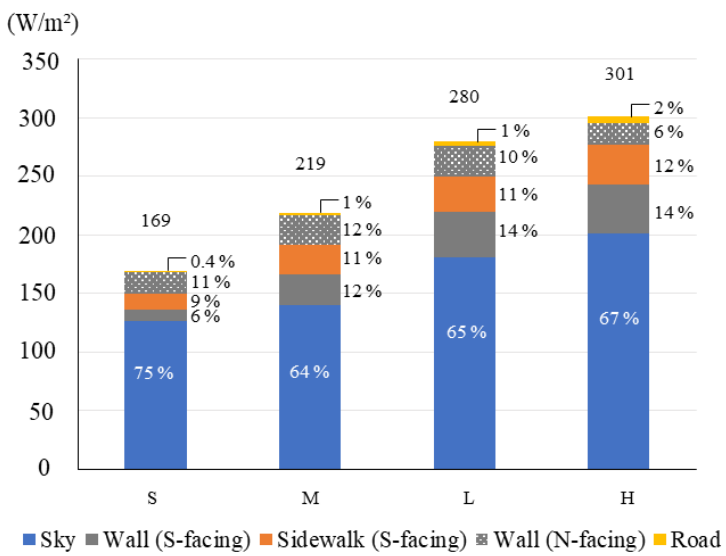

Fig. 20. The reduced amount of radiation incident on pedestrians from 5 elements due to trees. The ratio shows the percentage of each element occupied in the total reduction.

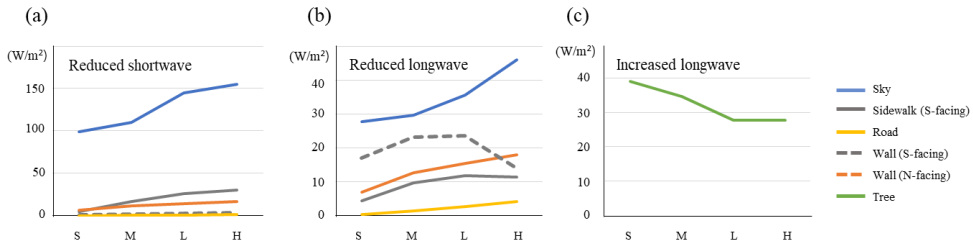

Fig. 21. The reduced amount of shortwave (a) and longwave radiation (b) incident on pedestrian from 5 elements and increased longwave radiation from trees (c).

Every element that has a surface temperature emits longwave radiation, including trees, as shown in Eq. (3) (Fig. 21). This amount of radiation offsets the reduction in shortwave radiation due to the trees (C. Y. Park et al., 2018). For this reason, if trees are not providing shade on pedestrians, they cannot reduce shortwave radiation and just emit longwave radiation and it could increase MRT. Therefore, planner should be careful that tree can provide shade to pedestrians.

3.3.3. Limitations

This study has some limitations because it simulates the tree's shading effect using a model that simplifies reality. Firstly, the model simulates the average value in one block. In a real S-facing sidewalk in a block, some spots wouldn't have shade if the tree shade occurs sparsely. Then, pedestrians under the shade of a tree have lower MRT while others may have higher MRT. In this study, however, MRT was averaged to a single value. Therefore, there is

a limit to not being able to detect the MRT change in a street. Secondly, the shape of tree has limitation. For ease of calculation, tree canopy has quadratic rectangular form as shown in Fig. 17 and the 2D domain also leads to a limitation in the use of the clumping factor. But in order to better reflect reality, trees are divided into 10 vertical layers that have different net radiation fluxes with by height. The clumping factor varies depending on the species on a micro scale and varies with the spacing between trees on a street scale. Therefore, calculating or measuring the clumping factor in a heterogeneous landscape is recommended (Q. Chen et al., 2008). This study has assumed that leaves are randomly distributed (clumping factor = 1). There is a need for further research to determine the clumping factor on a street scale and apply it to the cooling effect of trees.

Besides the tree variables, the street geometry and orientation also have a significant impact on the pedestrian MRT (Ali-Toudert & Mayer, 2006; Limor Shashua-bar & Hoffman, 2003). These two factors are also related to the angle between the incident solar radiation and the building wall. In summer, the sun rises from the east towards the north until noon, and then descends towards the west. For this reason, in streets oriented E–W, the shade is usually on the north side of buildings and trees. Pedestrians on the N-facing sidewalk are affected by the building geometry, while the others on the S-facing sidewalk are affected by the tree size. On streets oriented N–S, shade dominates the northwest of buildings or trees before noon, whereas after noon, it dominates the northeast. As both sidewalks in this case are mainly affected

by building shade, the shading effect due to trees would be low. Thus, this study examined only E–W streets, which are the most vulnerable to radiation exposure without trees (Holst & Mayer, 2011; Mayer et al., 2008; Takebayashi et al., 2014). Urban planners also need to be aware of this pattern.

Since the study used MMRT and focused on the shading effects of trees, storage heat flux and latent heat flux estimation for calculation of longwave radiation were simplified. Also, the evapotranspirational cooling effect of street trees was neglected. Future study can consider the total cooling effect of trees, including evapotranspiration effects. They can furthermore assess the total cooling effect of trees and calculate thermal comfort indices which factor in air temperature reductions, humidity changes, and wind speed changes (e.g., Krayenhoff et al., 2015) as well as mean radiant temperature reduction.

3.4. Conclusion

Planting trees in the street canyon is an effective strategy for reducing the urban radiation exposure of pedestrians. Trees provide shade by intercepting incident radiation such that it is not incident on pedestrians or nearby surfaces. In this study, pedestrian MRT was calculated by assessing the impacts of street tree spacing and tree size on solar (shading) and longwave radiation exchange. The results show that MRT decreases exponentially as the spacing between trees decreases. This is most apparent for small trees. When urban planners design street trees, they should consider the reduction slope and

choose an effective tree spacing for reducing radiation exposure. The results also show that tree size is more important than street size on the S-facing side of an E-W street. When the tree spacing is 11 m on a wide street, MRT reduction varies by 23.5 K between small trees (6 m tall & 3 m wide; 9.5 K MRT reduction) and large trees (22 m tall & 10 m wide; 33 K MRT reduction). The results also confirm that most of the MRT reduction results from the blocking of radiation from the sky. This is mostly due to interception of direct shortwave radiation from the sky. This process is also important for the nearby surfaces (walls and sidewalk) to reduce the reflected shortwave and emitted longwave radiations from those surfaces.

In conclusion, selecting an appropriate spacing between trees is important to improve thermal environments for pedestrians. If a planner chooses smaller trees, it is recommended they choose smaller tree spacing because MRT reduction effects increase exponentially with reduced spacing. On the other hand, if a planner chooses larger trees, they can increase the tree spacing larger trees with wide spacing more effectively reduce MRT than smaller trees with narrower spacing. This study can be beneficial for street design by providing information about optimal tree spacing, an important variable that can be chosen to reduce radiation exposure for pedestrians.

Acknowledgment

This work was supported by Korea Environmental Industry and

Technology Institute (KEITI) through Climate Change Response Technology Project, funded by Korea Ministry of Environment (MOE) (201800131002) and by the BK 21 Plus Project in 2019 (Seoul National University Interdisciplinary Program in Landscape Architecture, Global Leadership Program toward innovative green infrastructure).

IV. CHAPTER 3: Optimal multi-strategies modeling reveals a range of options for reducing pedestrian radiation exposure that integrate four strategies

4.1. Introduction

Urban warming can be a serious problem affecting the built environment. Reduced vegetation and increased construction in urban areas increases urban heat levels (C.-Y. Sun, 2011) which results in enhanced heat stress for urban residents, particularly pedestrians, due to their increased exposure to radiation heat flux (Lee & Mayer, 2018b; Rosso et al., 2018). Enhanced heat stress can affect human health, particularly among more vulnerable older people (Thorsson et al., 2014). There is also evidence that mortality and morbidity during heat extremes have increased due to climate change (Oudin Åström, Forsberg, Ebi, & Rocklöv, 2013). Especially significant warming occurs over the tropical and subtropical where most mega-cities are located (Golden, 2004) and this phenomenon exacerbate the problem of health and well-being. Therefore, improving the thermal environment of streets and reducing the radiation exposure of pedestrians has become an important research issue (C. Y. Park et al., 2018; C.-Y. Sun, 2011). Among the many potential strategies, planting trees or grass and converting surface albedos have been widely studied because they are realistic strategies involving lower costs than structural changes such as changing building orientation or aspect ratio. As

well as identifying the effect of options for reducing pedestrian radiation exposure, it is important to be able to select suitable strategies (Takebayashi et al., 2014).

Many previous studies have focused on single strategy for mitigating urban heat (Dimoudi et al., 2014; Djedjig et al., 2016; Napoli et al., 2016; Oliveira et al., 2011; Takebayashi & Moriyama, 2009). However, combining multiple strategies could result in different effects (E. Scott Krayenhoff et al., 2018); for example, there can be four different combination effects when planting a combination of trees and grass (Fig. 22). In some cases, the individual effects of different strategies can simply be merged (additive), or the combined effect may be larger than the sum of individual effects (synergistic). In other cases, one effect may be reduced (intersecting) or not be exhibited (overlapping) by combined plantings, resulting in a smaller combined effect. Because of this combination effect, researchers have tried to determine optimal combinations of strategies, such as green infrastructure and green pavements, using multiple scenarios (Battisti, Laureti, Zinzi, & Volpicelli, 2018; Limor Shashua-bar, Tsiros, & Hoffman, 2012; Yuan, Emura, & Farnham, 2017). Yuan et al. (2017) reported that a low wall albedo and some green area was the best combination among six scenarios with the combination of albedo and green area. Battisti et al. (2018) analyzed the effect of pavement and greening and found that combining two strategies (permeable green pavements plus cool roofs) could effectively mitigate heatwaves during the summer.

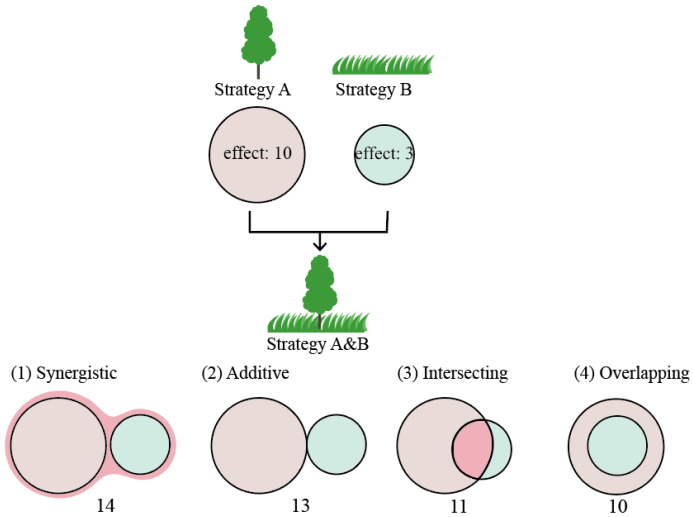

Fig. 22. Various combination effects of heat mitigation strategies

Although scenario research can effectively identify good options, it has limitations for searching multi-strategy options. Scenario research assesses options by considering key problems and identifying key alternatives (Peterson, Cumming, & Carpenter, 2003). In this process, three or four scenarios are usually selected as the study domain, whereas more than four can limit users' ability to explore uncertainty and may confuse them (Heijden, 1996; Peterson et al., 2003). This limitation of the number of scenarios makes it difficult to review the many possible combinations of conditions of multi-strategies. Optimization using meta-heuristics is another approach that has been used to solve such nonlinear problems (Hertz & Widmer, 2003), as it is flexible enough to handle many different combinations of problems (HassanzadehFard & Jalilian, 2016). Previously, optimization models have been shown to be effective decision support tools for solving real world problems in diverse fields (e.g., financial decision, building design, land use

allocation, road network, storm water management) by providing alternatives to decision makers (Evins, 2013; Gallo, D'Acierno, & Montella, 2010; Hochreiter & Pflug, 2007; Macro, Matott, Rabideau, Ghodsi, & Zhu, 2019; Mohammadi, Nastaran, & Sahebgharani, 2016). However, to our knowledge, no previous study has applied optimization using meta-heuristics to radiation exposure mitigation strategies. Since the radiant transfer process in urban area is complex and various drivers contribute to reduce radiant heat load, optimization with meta-heuristics should be applied to this field.

Another advantage of this optimization approach is that it can be utilized with multi-objective techniques (Jones, Mirrazavi, & Tamiz, 2002). Decision makers must consider cost effectiveness in order to provide the maximum effect within a limited budget, and they need information about the trade-offs between costs and effects (Macro et al., 2019). Such information can lead to effective planning assessments in two ways. First, decision makers can choose a plan that is appropriate for the available budget. If there are several plans that fall within the budget, they can select one with a higher benefit and lower cost. Second, plans may exist that have similar benefits and costs but different strategy combinations. In this case, information can be provided on alternatives to the best plan. Moreover, even if the best plan is the most cost effective, alternative plans can be chosen depending on the situation. Finding radiant fluxes mitigation plans considering both mitigation effect and cost can help decision makers decide better plans.

The primary goal of this study is to develop a model that can evaluate

multiple strategies for maximizing mean radiant temperature (MRT) reduction and minimizing cost. This study connected multi-objective optimization with a MRT simulator, which represents radiation exposure of pedestrians and plays a fundamental role in thermos-physiological concept for assessing thermal environment (Lee et al., 2013). It is also a critical variable to predict heat-related mortality (Thorsson et al., 2014). This study simulated an urban street canyon and evaluated the combined values of four modifications relating to tree and grass planting and changing the albedo of canyon walls and pavement using a MMRT (Multilayer MRT) model. The results identify a wide range of solutions to reduce heat-related mortality and develop thermally comfortable urban areas, dependent on the objectives and constraints that real world planners might have. This study will provide insights for sustainable urban planning under climate change.

4.2. Methods

Our model used an optimization algorithm that determines the decision variable of each strategy by considering two objectives: maximizing the radiant fluxes mitigation effect and minimizing costs. The model focuses on pedestrians in street canyons and radiant fluxes as the combined radiant heat load on a pedestrian (i.e., MRT). As the key strategies, this study selected four more realistic and lower cost options than changing the urban architectural geometry for reducing pedestrian MRT in a street canyon: street tree planting, grass planting, and albedo reduction of building walls or sidewalks. This

study combined these effects into a total MRT reduction effect for a pedestrian on a street. This study presents model tests of MRT reduction strategies using a hypothetical street canyon.

4.2.1. Maximizing MRT reduction

This study used MRT as the heat variable, which is the uniform temperature of an imaginary enclosure in which the radiant heat transfer from the human body equals the radiant heat transfer in an actual non-uniform enclosure (ASHRAE, 2001). MRT integrates the shortwave and longwave radiation flux densities emitted and reflected from a three-dimensional environment (Lee et al., 2013; Thorsson et al., 2007). Although MRT does not consider additional meteorological variables (air temperature, humidity, wind speed, and water vapor pressure) which determine the perception of heat by human, MRT shows the greatest impact on human thermal comfort during clear summer days (Lee et al., 2014). Moreover, MRT exhibits larger spatial variability, mainly due to the shadow patterns, thermal properties of surface materials, and the moisture status and effective variables for identifying hot spots of heat stress risk (Thorsson et al., 2014).

Calculating the MRT mitigation effect allows us to combine the effect of several strategies. The selected strategies are street tree planting (T), grass planting (G), albedo reduction of building walls (W), and sidewalks (S). These strategies were selected because they are relatively easy to apply

without changing the urban geometry and many previous studies have demonstrated their successful MRT mitigation effects (Klemm et al., 2015; Lee et al., 2016; Mayer et al., 2008; Salata, Golasi, Vollaro, & Vollaro, 2015; Takebayashi & Moriyama, 2009; Taleghani, Tenpierik, et al., 2014; Zeng & Dong, 2015; Zölch et al., 2016). The effects of these strategies on the energy balance of pedestrians in an urban street canyon are as follows:

- Strategy T (Fig. 23, ①): This has been the most widely used strategy for MRT mitigation (Klemm et al., 2015; Lee et al., 2016; Mayer et al., 2008; C. Y. Park et al., 2018; Zeng & Dong, 2015; Zölch et al., 2016). As trees intercept radiation, they can decrease the absorbed radiation densities of people in the same environment (Holst & Mayer, 2011; Lee et al., 2013). This effect is strongly dependent on the tree geometry (height, shape and width of the crown) (Lobaccaro & Acero, 2015). Greater tree coverage (leaf area density (LAD), leaf area index (LAI), number of trees) provides greater reduction of MRT in urban environments (Shashua-Bar, Tsiros, & Hoffman, 2010). In this study, trees are located between the sidewalk and the road. The decision variable is the number of trees.

- Strategy G (Fig. 23, ②): Green pavements have been compared with asphalt or other impervious pavement surfaces in many studies. Lee and Mayer, (2018b) found an averaged MRT reduction during 1000-1600 LST was 17.6 °C when the asphalt surface was changed to green pavement. Furthermore, the surface temperature of grass is lower than that of asphalt, block, wood, and concrete (D. Armson et al., 2012;

Takebayashi & Moriyama, 2009). Lower temperature surfaces emit lower longwave radiation, resulting in lower MRT. However, compared with low albedo impervious pavements (i.e., asphalt and some concrete), grass reflects more solar radiation to pedestrians (Takebayashi & Moriyama, 2009). If trees are planted on the grass, they can block the solar radiation and mitigate the reflection effect, indicating that shaded grass has a better cooling effect than a sunlit grass area (D. Armson et al., 2012). Therefore, Lobaccaro and Acero (2015) have emphasized that grass under trees is an effective strategy for reducing heat stress along streets. This study defines strategy G as a grass planting on the sidewalk adjacent to the road. The decision variable is the area of the grass (m2).

- Strategy W and S (Fig. 23, ③ and ④): In street canyons, the surfaces that predominantly affect people are the building walls and sidewalks. Previous studies have suggested that a higher albedo could reflect substantial radiation and reduce urban heat. Increasing the roof albedo is an effective way of reducing the net shortwave radiation in urban areas (Li, Bou-Zeid, & Oppenheimer, 2014; Yang, Wang, & Kaloush, 2015). In addition, High albedo materials inside the canyon were found to reduce air temperature of urban canyon (Erell et al., 2014). However, recent research has revealed that a higher albedo within an urban street environment (i.e., building walls and sidewalks) can have negative effects on radiant pedestrians thermal exposure (Lee & Mayer, 2018b; Salata et al., 2015; Taleghani, Tenpierik, et al., 2014). This is because higher

albedo surfaces will reflect more incoming shortwave radiation onto people, increasing radiation flux densities (Lee & Mayer, 2018b). In addition to heat, high albedo pavements may have adverse effects such as greater slip risks or causing visual interference due to increased light levels (Richard, Doré, Lemieux, Bilodeau, & Haure-touzé, 2015). Strategy W and S therefore involves reducing the albedo of walls and sidewalks to reduce the radiant flux densities of pedestrians. In appendix C, the study reviewed the albedo ranges for building wall and sidewalk materials. The decision variable is the area of the new material surface (m2).

Our model focuses on the most cost effective street design changes and does not involve geometric changes. MRT reduction effects of four strategies are calculated using MMRT model. The MMRT model calculates pedestrians' MRT in a complex street canyon with trees considering vertical heterogeneity, with simple input data a low time consuming (C. Y. Park et al., 2018). This model represents radiation exchange in a complex street canyon, particularly with respect to its attenuation by green infrastructure, using Monte Carlo ray tracing. The model needs four categories of input data: date and time, latitude and longitude, meteorological, geometric data. Users also can control the thermal parameter such as albedo and emissivity. Fig. 23 shows how the strategies can be applied to the MMRT model. Parameters including tree height, tree crown width, width and height of grass, and material albedo must be set in order to operate the optimization model. For the model test, this study

sets default values for input data, described in section 2.4.

The model was further developed the leaf surface temperature estimation using latent heat loss in the leaf energy budget from air temperature, vapor deficit, and conductance (Campbell & Norman, 1998). But, heat conductance relates to the wind speed estimate is still simplified to reduce computational expense.

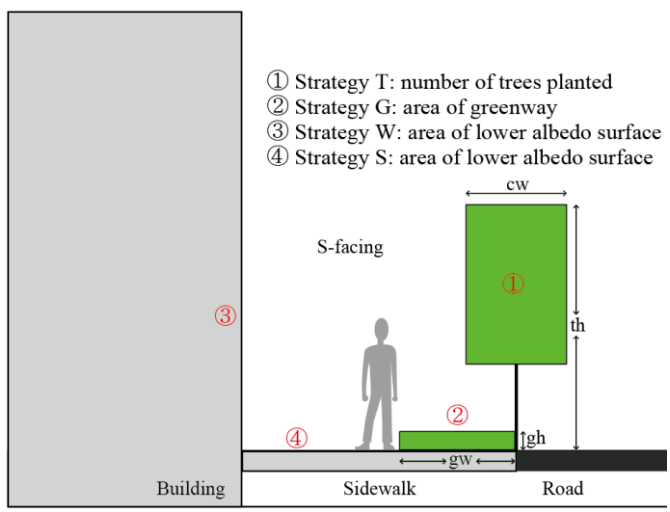

Fig. 23. Illustration of MRT mitigation strategies and variables used in the model for the south-facing side of the street: cw = canopy width, th = tree height, gw = greenway width, gh = height for grass.

The model calculates pedestrian MRT considering changes of four strategies decision variables, and includes their combination effects (Eq. 27). $MRT_{Strategies}$ means the average MRT of the pedestrian who walk on the

middle of the entire south-facing sidewalk.

$$MRT_{Strategies} = f_{MMRT}(\mathrm{T}_{number}, G_{area}, W_{area,} S_{area}) \quad (27)$$

Here, T_{number} is the number of trees planted, G_{area} is the area of grass planted, and W_{area} and S_{area} are the area of lower albedo surfaces of building walls and sidewalks. MRT reduction describes how much the MRT is reduced by strategies compared to a 'no strategy' condition at maximum MRT (Eq. 28).

$$MRT\ mitigation\ (benefit) = MRT_{NoStrategy} - MRT_{strategies} \quad (28)$$

4.2.2. Cost minimization

This study considers costs twice in the model. First, the study sets a budget (maximum cost) as a constraint factor because urban development and planning typically have limited budgets. This constraint factor ensures that the results do not exceed the budget. Second, one of the optimization objectives is to minimize the cost; therefore, the model aims to find plans that cost as little as possible within the budget. This study consider the implementation cost of the four strategies by multiplying the decision variables by the unit cost of each strategy (Eq. 29).

$$Cost = T_{number}Cost_T + G_{area}Cost_G + W_{area}Cost_W + S_{area}Cost_S \quad (29)$$

Where $Cost_T$ is the cost for one street tree and $Cost_G$, $Cost_W$, and $Cost_S$ are the costs for 1 m2 of grass, converted wall, and converted sidewalk,

respectively. Tree and grass planting generally entails two or three years of maintenance as well as construction. Therefore, when the model calculate the unit cost of strategy T and G, it also considers maintenance work such as pruning, fertilization, and weeding. These unit costs vary depending on the specific type of strategy (e.g., the type of tree or material).

4.2.3. Optimization model

The optimization model developed in this study aims to identify the optimal combination of four heat mitigation strategies in order to achieve the MRT mitigation goal at low cost. The objective of this model is to provide the decision maker with a wide range of strategy combinations.

The strategy combination was optimized using a non-dominated sorting genetic algorithm II (NSGA II), which produces Pareto optimal solutions using the non-domination rank and crowding distance (Deb, Pratap, Agarwal, & Meyarivan, 2002; Yoon, Kim, & Lee, 2019). It contains sets of priorities considered as a range of values quantifying the trade-off between different objectives; i.e., the benefit (MRT mitigation) and the cost (Woodward, Kapelan, & Gouldby, 2014; W. Wu et al., 2016).

Considering the budget constraint value, this study randomly created N initial plans (parent generation) for the searching space beyond existing knowledge. Then, by selection, crossover, and mutation, new N plans were created (children generation). To prevent the loss of good solutions, this study

combined previous plans and new plans (elitism) and selected the next generation using the nominated rank and crowding distance. Finally, after a number of iterations of the main loop (selection, crossover, mutation, and elitism), this study obtained the Pareto optimal plans (Fig. 24). The population size (N) and number of iterations (M) were selected as 70 and 80 respectively by repetitive pilot test (Appendix C). Because a large number of Pareto optimal plans are identified by the optimization model, it is necessary to reduce this number to a smaller, more manageable ideal set of plans for the decision maker (W. Wu et al., 2016). In this way, this study can provide ideal plans targeting MRT risk reduction and compare alternative plans with similar benefits and costs.

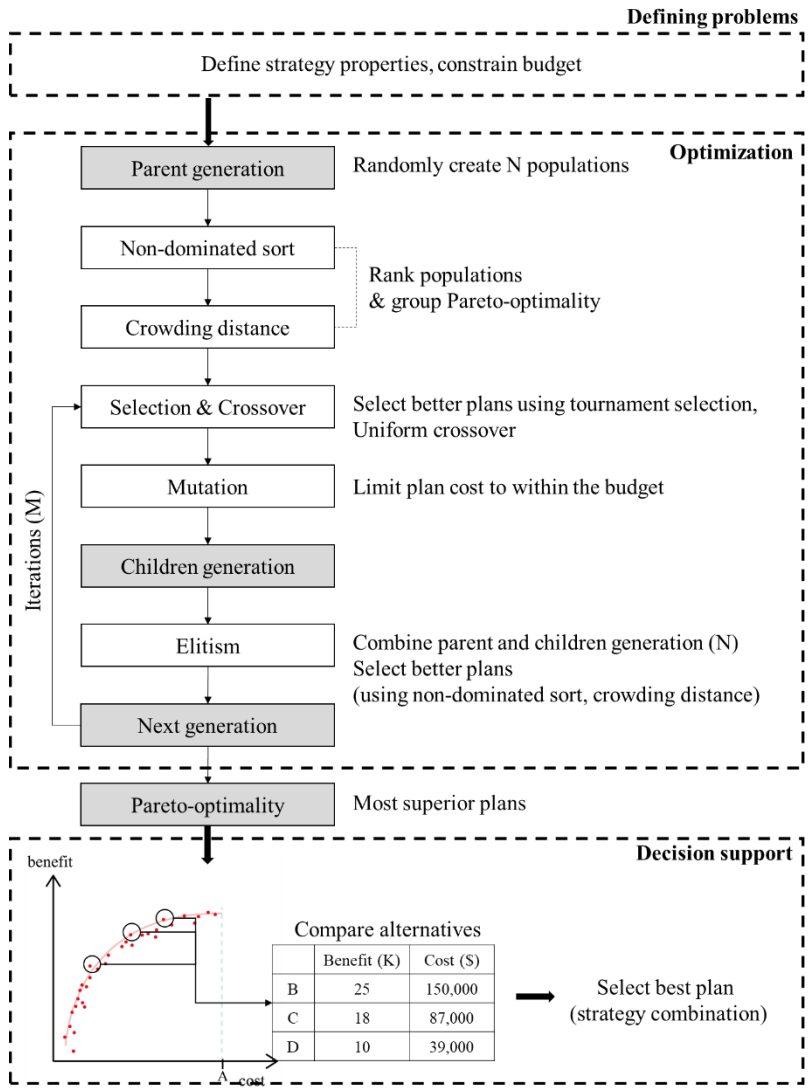

Fig. 24. Optimization process for determining optimal plans.

4.2.4. Model test site

To emphasize the optimal results, this study used a hypothetical study site

with realistic geometry; i.e., a street canyon with six car lanes. Table. 1 shows the input data for model test. The sidewalk width is 5 m and the street length is 400 m (Fig. 25). Overall, the aspect ratio (height-to-width ratio, H/W) of street canyon is 0.67. The orientation of the street is east-west, so that the south facing pedestrian receives significant quantities of direct solar radiation (Nakamura & Oke, 1988). The temporal target was the daily maximum MRT during clear days (cloud fraction under 50%) in June–August 2017. Since the heat mortality was related with daily maximum MRT (Thorsson et al., 2014), this study chose the time target as the time with the highest MRT of the day. The target time can be changed according to the purpose of the plan (e.g., reducing mortality risk). In order to reduce the simulation time, the study used one time target (maximum MRT time of the average day during June to August). The average value of daily air temperature and dew point temperature data from the Korea Meteorological Administration. Therefore, the final time variables were as follows. The date was DOY 179 (28th June), and the time was 1300 local standard time (LST) (highest MRT of the day).

Before implementing the heat mitigation plans, the site contained 10 gingko biloba trees and no grass. The albedo of the walls and sidewalk was 0.8 (polished white granite). The parameters of the four strategies were shown in Table 3. The strategies costs used the 2018 Korean landscape architecture standard statement (KSLA, 2018) and 2016 Land and Housing guide specifications (LH, 2016) which include the cost of materials, labor, and other expenses. $Cost_W$ and $Cost_S$ include installation cost. But $Cost_T$ and

$Cost_G$ include three years of maintenance costs as well as installation cost.

The albedo range of building wall and sidewalk pavement are 0.2-0.9 and 0.1-0.8 respectively (Appendix C). In order to maximize the effect of albedo reduction, this study used the albedo of the polished white granite (0.8), which was used as open space pavement (Shahidan, Jones, Gwilliam, & Salleh, 2012), as the origin surface albedo.

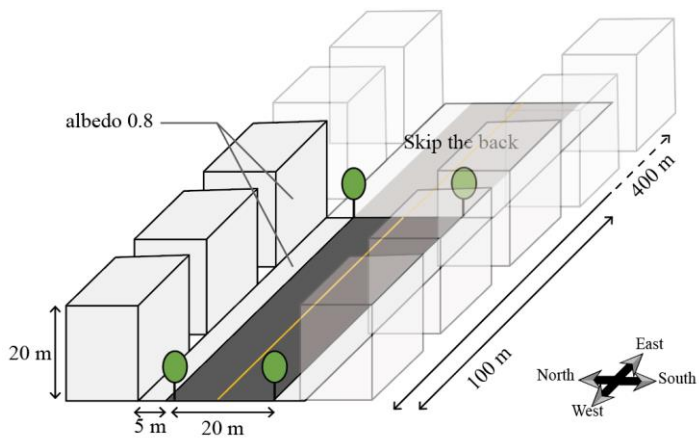

Fig. 25. Illustration of the hypothetical study site.

Table 3. Input data of the model.

Categories		Parameter	Cost ($)
Geometric data	Longitude and latitude (°)	126.9, 37.6	-
	Street orientation (°)	90	-
	Building height and width (m)	20, 5	-
	Road width (m)	20	-

Meteorological data	DOY and LST	179, 1300	-
	Air temperature (℃)	29.2	-
	Relative humidity (%)	37.2	-
	Vapor pressure (hPa)	15	-
Strategies	T: Tree height and canopy width (m)	7, 5	4,749/tree
	G: Grass height and greenway width (m)	0.3, 1.5	51/m^2
	W & S: Reduction of albedo (wall & sidewalks)	0.8 to 0.3	181/m^2, 149/m^2

After simulating the optimization model, this study applied the mortality risk level developed by Thorsson et al. (2014). This risk level from the mortality data in Stockholm, Sweden where the average air temperature during July is 22 ℃. A specific target goal or criterion can help with the plan selection (Woodward et al., 2014). They divided the daily maximum MRT level into three, where level 1 indicates a 0–5% mortality risk increase (from 320.75–328.15 K), level 2 indicates a 5–10% mortality risk increase (from 328.15–330.55 K), and level 3 indicates a severe mortality risk increase of over 10% (over 330.55 K). This study divided the Pareto optimal plans according to the risk level in order to support the decision making process.

4.3. Results

4.3.1. Range of optimal solutions

The model identified 48 Pareto optimal plans (Fig. 26), which exhibit the trade-off between MRT reduction and costs; i.e., an increase in the benefit leads to a higher implementation cost. The plan with the highest benefit (1) results in an MRT reduction of 21.6 K (the average reduction MRT of pedestrian who walk on the middle of the entire south-facing sidewalk) and costs $199,968. The cheapest plan (9) only exhibits a 0.9 K reduction and costs $5,610. The benefit gap of 20.7 K results in a cost change of $194,358. Therefore, decision makers can choose an appropriate plan by considering the trade-off between the two objectives. The no strategy condition exhibited an MRT of 342.9 K at 1300 LST, which equates to risk level 3. This can be reduced to level 2 or 1 by reducing the MRT by 10.4 K or 14.3 K, respectively. Plan 6 and 5 are the lowest cost plans that satisfy the MRT reduction to level 2 and level 1, respectively (Table 4). This indicates that spending $118,725 on radiation exposure reduction strategies can reduce the mortality risk by over 5% (level 1) and an additional $88,734 can reduce the mortality risk by over 10% (level 2).

The Pareto optimality can provide decision makers with alternatives that involve different strategies but produce similar effects. For example, plan 6 and 7 have very similar benefits and costs (Table 4). However, compared with plan 6, plan 7 involves a smaller grass area and additional albedo changes in the wall and sidewalk. These alternative options are a substantial advantage as they provide different opportunities. If urban planners prefer more grass in the street, they can select plan 6. If the street is not appropriate for planting

much grass on the sidewalk, they can select plan 7.

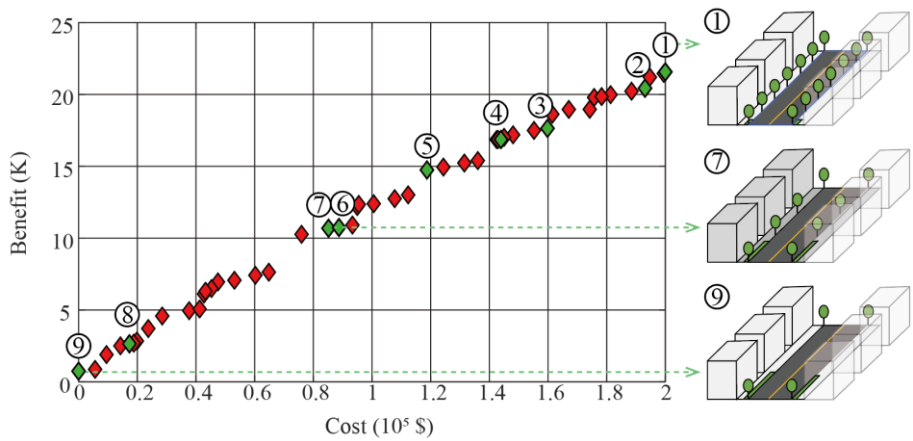

Fig. 26. Pareto optimal plans (red) and example plans 1–9 (green). Plans 1, 7, and 9 are illustrated as 100-m long sites.

4.3.2. Strategy combinations

The model results represent the optimal strategy combinations for MRT reduction and every plan includes the decision variables of the four strategies: T, G, W, and S. Most Pareto optimal plans combine T and G and only some include W and S (Fig. 27). Plan benefits increase with an increasing number of trees, which indicates that MRT mitigation is mainly affected by the number of trees (strategy T). However, the expense costs of trees also increase total costs of plans. Therefore, the ability of tree planting can dominate the urban planning for mitigating MRT. For an equal number of trees, the benefit

increases with increasing grass area, which infers that grass planting (strategy G) is the next most cost-effective strategy.

Strategies W and S were selected less frequently because of their low benefit-cost ratio. Even though G, W, and S have similar MRT mitigation benefit, W and S need higher costs ($181/m2, $149/m2) than G ($51/m2). When the study applies 100% of G (1200m2), W (15000m2), and S (4000m2) in the study site, the MRT reduction benefits are 2 K, 5.7 K, and 6.6 K respectively. However, when the study compared this benefit with cost, the ratios (K/$1,000,000) are 32.8, 2.1, and 11.1. This cost-effectiveness would have influence on the Pareto optimal plans. However, if an urban planner chooses inexpensive method such as painting to change the albedo of walls and sidewalks, the Pareto optimal plans would also include W and S. That is, the strategy combination results will differ according to the strategy parameters (e.g., size, available area, and thermal parameter) and cities with different unit costs.

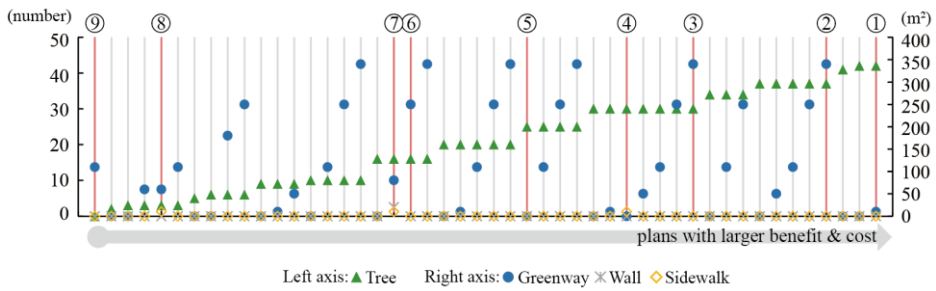

Fig. 27. Figure 28. Decision variables (T, G, W, and S) of all Pareto optimal plans against the size of plan benefits (left Y-axis shows the implemented size for strategy T and right Y-

axis shows that for strategy G, W, and S). Red lines indicate plans 1–9.

The benefit values of the optimal plans represent their combined effects on MRT mitigation. When comparing individual and combined strategy effects, this study notes that these strategy combinations exhibit synergistic effects. Table 4 shows the combination effect of selected nine plan, which are representative combinations among Pareto optimal plans. They have 0.3 to 0.6 K synergistic effect except for singular strategy plan (plan three and five). These synergistic effect values are small compared to the total benefit, but they are large enough to change the order of combinations' benefit. In other words, the multi-strategies model considers the combination effects of strategies and provide decision makers planning options based on accurate estimates. Since the results in Table 4 are some part of the combinations, this study cannot know whether all multi-strategies for MRT reduction have synergistic effect. This study can say that the combination of T and G, or S, or W is more effective than applying single strategy.

Table 4. Description of the selected plans shown in Fig. 26 and their combination effects.

Plan (#)	Decision variable				Benefit (K)	Sum of single benefits	Synergistic combination effect	Cost ($)
	Tree (number)	Grass (m^2)	Wall (m^2)	Sidewalk (m^2)	(A)	(B)	(A-B)	
1	42	10	0	0	21.6	21.2	0.4	199,968
2	37	340	0	0	20.4	20.1	0.3	194,709
3	30	340	0	0	17.6	17.1	0.5	159,810
4	30	0	0	10	16.9	16.5	0.4	143,960
5	25	0	0	0	14.7	-	-	118,725

6	16	250	0	0	10.7	10.2	0.5	88,734
7	16	80	20	10	10.7	10.1	0.5	85,174
8	3	60	0	10	2.7	2.1	0.6	18,797
9	0	11.	0	0	0.9	-	-	5,610

4.4. Discussion

4.4.1. Decision support tool for urban planning

Since decision makers have different objectives and design constraints, this study was designed to provide a wide range of alternatives. First, for satisfying varying objectives, multi-objective (benefit and costs) Pareto was provided. Decision makers can select option which more reflect their preference among MRT reduction benefit and low cost. If decision makers prefer high benefit, they can select from plans 1-5 that can reduce mortality risk to level 1. On the other hand, if decision makers consider minimum cost, they can select lower benefit and cost plans. The alternatives with similar benefits and costs but different combination of strategies (e.g., plan 6 and 7) permit decision makers to take account of their design preference or site condition. In addition, since many people are involved in the decision making process, having quantitative evidence on strategies' effect is effective in gathering feedback. This study selected relatively economical strategies and there were no construction changes. But if more expensive reconstruction can be considered, plans with structural changes such as building orientation or aspect ratio can further reduce MRT (Ali-Toudert & Mayer, 2006; Johansson & Emmanuel, 2006; Ketterer & Matzarakis, 2014; Lin, 2009; Lobaccaro & Acero, 2015)

The multi-objective optimization model can consider additional objective or replace them for other objectives. Even though this study is focusing on the summer, urban planner should consider the effect of four strategies in other seasons. In particular, since the winter in Seoul, Korea is cold, they should notice the adverse effects of MRT reduction strategies in winter. Lowering albedo can reduce MRT by lowering reflected radiation to the pedestrian. However, green infrastructures would not have a significant impact because they do not have leaves in winter. The consideration of other season can be another objective in the model. Other objective s which are not associated with MRT also can be accommodate for finding optimal urban plans. For example, Yoon et al. (2019) proposed a planning model to determine the location and type of green areas based on cooling effect and connectivity. Macro et al. (2019) also used optimization tool to find out the proper green infrastructure investment by minimizing the combined sewer overflows and minimizing the cost. For solving the water supply issue, Wu et al. (2016) showed the preferred multi-objective such as minimizing the total life cycle cost, maximizing the volumetric reliability of water supply or storage targets in the reservoirs.

4.4.2. Strategy combinations for MRT mitigation

This study observed a combination effect in the MRT reduction strategies. Plans with combination of tree and other strategies showed a synergistic combination effect. This effects might be come from the lowering surface

(grass/sidewalk) temperature due to tree shade. When the study simulates the surface temperature of grass/sidewalk in the case of grass/sidewalk only (1) and the case of combining with tree (2), case (2) shows lower surface temperature. The lower surface temperature emit lower longwave radiation to the pedestrian, which results in additional MRT reduction effect. In addition, tree shade reduce incident solar radiation into grass/sidewalk/wall, which result in reducing reflected shortwave radiation from those surfaces. Middel and Krayenhoff (2019) also found that grass with trees could be better options for thermal comfort and reducing MRT due to this synergistic effect based on in-situ measurement. To our knowledge, no previous heat mitigation strategy research has discovered this combination effect, which could result in misleading information for urban planners implementing heat mitigation strategies. In general, it is difficult to achieve the desired heat reduction effect using only one strategy; therefore, planners need to apply multiple strategies in one location (Battisti et al., 2018; Zölch et al., 2016). If the planner only considers the individual strategy effects, they are likely to overestimate or underestimate the total effect of these various strategies. Our proposed strategy combination model can therefore help avoid erroneous estimates and establish a more appropriate plan whose exact benefits can be determined.

4.4.3. Next steps

The current study was limited by time scale, study site, computation dimension, and literature review. I believe that future studies will expand this

methods and overcome the limitations. For planning applications, users could run our model by adjusting only a few variables. If more types of strategy are developed and their effects are calculated in the MRT model, this optimization model can become more widely applicable and can better support urban planning decision making in order to reduce urban radiation exposure.

First, there are some limitation in the time scale and site geometry. This model test targets daily maximum MRT reduction at 1300 LST and a specific geometry street canyon. However, targeting time and site geometry is important parameter to affect to MRT. First, the timing of the highest MRT reduction effect differs between strategies. In the case of tree planting, as trees intercept incident solar radiation, times of strong solar radiation (approximately 1100–1300 LST) exhibit the highest MRT reduction effect (Park et al., 2018). However, lowering the surface albedo (dark brick albedo = 0.1) reduces the MRT in the afternoon (~1800 LST) when the surface is exposed to solar radiation, with the maximum effect appearing at 1500 LST (Taleghani et al., 2014). Therefore, the combination effect can vary depending on the time. Currently, because of the time consumed by MRT simulation, producing an optimization time series would require an enormous amount of time. However, an important next step is to study heat mitigation strategies that incorporate combination effects over time. The site geometry can change the pedestrian MRT by controlling the building shade. As the hypothetical study site was determined as an east-west orientation and 0.67

aspect ratio, there was no building shade on the south facing sidewalk at 1300 LST. This structure provided high MRT of south facing pedestrian. Changing orientation to north-south or increasing aspect ratio would reduce large amount of MRT by adding building shade on the pedestrians. As well as street structure, the location of pedestrian affect to MRT. This results are about the pedestrian who walk on the middle of the south facing sidewalk. If pedestrians walk near the building, building wall albedo could be an important strategy because they are highly influenced by the reflecting radiation from the walls. According to the characteristics and structure of street, researchers or urban planners can control such variables (i.e., street orientation, aspect ratio, pedestrian location) in order to apply this model to other sites.

Second, The MMRT model calculated the average MRT using 2D domain which is the compressed result of 3D street block (Park et al., 2018). This study chose the block scale decision variables (total number, total area) of the MRT reduction strategies because this study focused on the average MRT of street block. If researcher connect 3D domain model such as ENVI-met and SOLWEIG with optimization model what this study propose, they will able to extend the decision variables to 3D variable such as the location and shape of the strategy. However, 3D models has high computational cost, which makes hard to associate with optimization model. In order to support decision making, a model that can provide solutions repetitively and immediately is needed.

Third, there is few literature which studied the heat risk level and MRT. This study used mortality risk level to facilitate their selection which is studied in Stockholm, Sweden. Even though the study site of mortality risk level, Stockholm, Sweden, had similar maximum MRT value with Seoul, applying this criteria should be carefully considered in the study. To apply the risk level for other sites which have various conditions including MRT, more studies should discover the relationship between MRT and mortality risk in various cities in the future.

In addition, this study focuses on the current situation, whereas future research should study long-term MRT mitigation plans. Climate change is expected to increase heat mortality and heat related costs in the future (Ohashi et al., 2016; Wondmagegn et al., 2019). Some long-term urban planning studies have already been conducted in other fields. For example, Erfani et al. (2018) evaluated water supply planning using a multi-stage scenario tree, which provided strategies that had to be applied over time. It is vital to determine how future climate change will affect MRT and how we can deal with it.

4.5. Conclusions

The multi-strategies model focusing MRT reduction and green infrastructure will make the city sustainable. Since MRT is expected to increase due to climate change, this research has important applications for

mitigating heat related mortality under future climate change. MRT reduction would lead to save additional health-related costs by reducing the mortality risk. This study also found that most optimal options included planting trees and grass because they are cost effective strategies. These green infrastructures have diverse co-benefits and promote urban area to adapt to and mitigate against climate change, enhance sustainability and improve human health and well-being.

Acknowledgment

This work was supported by Korea Environmental Industry and Technology Institute (KEITI) through Climate Change Response Technology Project, funded by Korea Ministry of Environment (MOE) (201800131002) and by the BK 21 Plus Project in 2019 (Seoul National University Interdisciplinary Program in Landscape Architecture, Global Leadership Program toward innovative green infrastructure)

V. Conclusions

Reducing MRT is important for reducing heat mortality and improving well-being in the urban area. However, there is a lack of decision support tool for planning thermal-friendly urban street where pedestrians receive less radiant heat load. The study proposed three steps decision support tools based on physical radiation transfer model. Chapter 1 presented MMRT model which can be a base model for chapter 2 and 3. Even there are some limitations such as two dimension domain and simplified conductance, this model can represent pedestrian MRT who in the complex urban area with green infrastructure with a low time consuming. Chapter 2 provided quantified MRT reduction values depending on street tree size and their interval. The results show how much street tree which selected by urban planner can reduce MRT and help urban planner change the size or interval for satisfying their desired MRT reduction. Chapter 3 proposed the optimization method for obtaining multi-strategies combination plans satisfying two objectives: maximizing MRT reduction and minimizing cost. This method can provide a range of options and alternatives that help decision maker choose best option closest to their preference.

This study has gone some way towards enhancing our understanding of thermally-friend urban planning using decision support tool. This methods can be expanded to other objectives and strategies. This could eventually lead to sustainable development considering urban problem (e.g., heat mortality, urban flooding) due to urbanization and climate change.

VI. Bibliography

Abreu-Harbich, L. V. de, Labaki, L. C., & Matzarakis, A. (2015). Effect of tree planting design and tree species on human thermal comfort in the tropics. *Landscape and Urban Planning*, *138*, 99–109. https://doi.org/10.1016/j.landurbplan.2015.02.008

Alchapar, N. L., Correa, E. N., & Cantón, M. A. (2014). Classification of building materials used in the urban envelopes according to their capacity for mitigation of the urban heat island in semiarid zones. *Energy and Buildings*, *69*, 22–32. https://doi.org/10.1016/j.enbuild.2013.10.012

Ali-Toudert, F., & Mayer, H. (2006). Numerical study on the effects of aspect ratio and orientation of an urban street canyon on outdoor thermal comfort in hot and dry climate. *Building and Environment*, *41*(2), 94–108. https://doi.org/10.1016/j.buildenv.2005.01.013

Allen, R. G., Pereira, L. S., Raes, D., Smith, M., & Ab, W. (1998). *Crop evapotranspiration - Guidelines for computing crop water requirements - FAO Irrigation and drainage paper 56*. Rome: FAO. https://doi.org/10.1016/j.eja.2010.12.001

Armson, D., Stringer, P., & Ennos, A. R. (2012). The effect of tree shade and grass on surface and globe temperatures in an urban area. *Urban Forestry and Urban Greening*, *11*(3), 245–255. https://doi.org/10.1016/j.ufug.2012.05.002

Armson, David, Rahman, M. A., & Ennos, A. R. (2013). A Comparison of the Shading Effectiveness of Five Different Street Tree Species in Manchester , UK. *Arboriculture & Urban Forestry*, *39*, 157–164.

ASHRAE. (2001). *ASHRAE Fundamentals Handbook 2001 (SI Edition) American Society of Heating, Refrigerating, and Air-Conditioning Engineers*.

Battisti, A., Laureti, F., Zinzi, M., & Volpicelli, G. (2018). Climate mitigation and adaptation strategies for roofs and pavements: A case study at Sapienza University Campus. *Sustainability*, *10*, 1–20. https://doi.org/10.3390/su10103788

Brown, R. D., Vanos, J., Kenny, N., & Lenzholzer, S. (2015). Designing

urban parks that ameliorate the effects of climate change. *Landscape and Urban Planning*, *138*, 118–131. https://doi.org/10.1016/j.landurbplan.2015.02.006

Bruse, M., & Fleer, H. (1998). Simulating surface-plant-air interactions inside urban environments with a three dimensional numerical model. *Environmental Modelling and Software*, *13*(3–4), 373–384. https://doi.org/10.1016/S1364-8152(98)00042-5

Campbell, G. S., & Norman, J. M. (1998). *An introduction to environmental biophysics*. *Springer*. New York: Springer. https://doi.org/10.2307/4589381

Chen, Q., Baldocchi, D., Gong, P., & Dawson, T. (2008). Modeling radiation and photosynthesis of a heterogeneous savanna woodland landscape with a hierarchy of model complexities. *Agricultural and Forest Meteorology*, *148*(6–7), 1005–1020. https://doi.org/10.1016/j.agrformet.2008.01.020

Chen, Y. C., Tan, C. H., Wei, C., & Su, Z. W. (2014). Cooling effect of rivers on metropolitan Taipei using remote sensing. *International Journal of Environmental Research and Public Health*, *11*(2), 1195–1210. https://doi.org/10.3390/ijerph110201195

Coutts, A. M., White, E. C., Tapper, N. J., Beringer, J., & Livesley, S. J. (2016). Temperature and human thermal comfort effects of street trees across three contrasting street canyon environments. *Theoretical and Applied Climatology*, *124*, 55–68. https://doi.org/10.1007/s00704-015-1409-y

De, B., & Mukherjee, M. (2017). Optimizing Street Canyon Orientation for Rajarhat Newtown, Kolkata, India. *Environmental and Climate Technologies*, *21*(1), 5–17. https://doi.org/10.1515/rtuect-2017-0012

Deb, K., Pratap, A., Agarwal, S., & Meyarivan, T. (2002). A fast and elitist multi-objective genetic algoritm:NSGA -II. *IEEE Transactions on Evolutionary Computation*, *6*(2), 182–197. https://doi.org/10.1109/4235.996017

Dervishi, S., & Mahdavi, A. (2012). Computing diffuse fraction of global horizontal solar radiation: A model comparison. *Solar Energy*, *86*(6), 1796–1802. https://doi.org/10.1016/j.solener.2012.03.008

Dimoudi, A., Zoras, S., Kantzioura, A., Stogiannou, X., Kosmopoulos, P., &

Pallas, C. (2014). Use of cool materials and other bioclimatic interventions in outdoor places in order to mitigate the urban heat island in a medium size city in Greece. *Sustainable Cities and Society, 13*, 89–96. https://doi.org/10.1016/j.scs.2014.04.003

Djedjig, R., Bozonnet, E., & Belarbi, R. (2016). Modeling green wall interactions with street canyons for building energy simulation in urban context. *Urban Climate*, *16*, 75–85. https://doi.org/10.1016/j.uclim.2015.12.003

Du, H., Song, X., Jiang, H., Kan, Z., Wang, Z., & Cai, Y. (2016). Research on the cooling island effects of water body: A case study of Shanghai, China. *Ecological Indicators*, *67*, 31–38. https://doi.org/10.1016/j.ecolind.2016.02.040

Erbs, D. G., Klein, S. A., & Duffie, J. A. (1982). Estimation of the diffuse radiation fraction for hourly, daily and monthly-average global radiation. *Solar Energy*, *28*(4), 293–302. https://doi.org/10.1016/0038-092X(82)90302-4

Erell, E., Pearlmutter, D., Boneh, D., & Kutiel, P. B. (2014). Effect of high-albedo materials on pedestrian heat stress in urban street canyons. *Urban Climate*, *10*, 367–386. https://doi.org/10.1016/j.uclim.2013.10.005

Erfani, T., Pachos, K., & Harou, J. J. (2018). Real-Options Water Supply Planning: Multistage Scenario Trees for Adaptive and Flexible Capacity Expansion Under Probabilistic Climate Change Uncertainty. *Water Resources Research, 54*, 5069–5087. https://doi.org/10.1029/2017WR021803

Evins, R. (2013). A review of computational optimisation methods applied to sustainable building design. *Renewable and Sustainable Energy Reviews, 22*, 230–245. https://doi.org/10.1016/j.rser.2013.02.004

Feyisa, G. L., Dons, K., & Meilby, H. (2014). Efficiency of parks in mitigating urban heat island effect: An example from Addis Ababa. *Landscape and Urban Planning, 123*, 87–95.

Foudi, S., Spadaro, J. V., Chiabai, A., Polanco-Martínez, J. M., & Neumann, M. B. (2017). The climatic dependencies of urban ecosystem services from green roofs: Threshold effects and non-linearity. *Ecosystem Services, 24*, 223–233.

https://doi.org/10.1016/j.ecoser.2017.03.004

Gallo, M., D'Acierno, L., & Montella, B. (2010). A meta-heuristic approach for solving the Urban Network Design Problem. *European Journal of Operational Research*, *201*(1), 144–157. https://doi.org/10.1016/j.ejor.2009.02.026

Golden, J. S. (2004). The Built Environment Induced Urban Heat Island Effect in Rapidly Urbanizing Arid Regions – A Sustainable Urban Engineering Complexity. *Environmental Sciences*, *1*(4), 321–349. https://doi.org/10.1080/15693430412331291698

Grimmond, C. S. B., Cleugh, H. A., & Oke, T. R. (1991). An objective urban heat storage model and its comparison with other schemes. *Atmospheric Environment*, *25*(3), 311–326.

Grimmond, C. S. B., & Oke, T. R. (2002). Turbulent Heat Fluxes in Urban Areas: Observations and a Local-Scale Urban Meteorological Parameterization Scheme (LUMPS). *Journal of Applied Meteorology*, *41*(7), 792–810. https://doi.org/10.1175/1520-0450(2002)041<0792:THFIUA>2.0.CO;2

Gros, A., Bozonnet, E., & Inard, C. (2011). Modelling the radiative exchanges in urban areas: A review. *Advances in Building Energy Research*, *5*(1), 163–206. https://doi.org/10.1080/17512549.2011.582353

HassanzadehFard, H., & Jalilian, A. (2016). A novel objective function for optimal DG allocation in distribution systems using meta-heuristic algorithms. *International Journal of Green Energy*, *13*(15), 1624–1634. https://doi.org/10.1080/15435075.2016.1212355

Heijden, K. van der. (1996). *Scenarios: the art of strategic conversation*. *Wiley*. New York.

Hendel, M., Parison, S., Grados, A., & Royon, L. (2018). Which pavement structures are best suited to limiting the UHI effect? A laboratory-scale study of Parisian pavement structures. *Building and Environment*, *144*(June), 216–229. https://doi.org/10.1016/j.buildenv.2018.08.027

Hertz, A., & Widmer, M. (2003). Guidelines for the use of meta-heuristics in combinatorial optimization. *European Journal of Operational Research*, *151*(2), 247–252. https://doi.org/10.1016/S0377-2217(02)00823-8

Hochreiter, R., & Pflug, G. C. (2007). Financial scenario generation for stochastic multi-stage decision processes as facility location problems. *Annals of Operations Research*, *152*(1), 257–272. https://doi.org/10.1007/s10479-006-0140-6

Holst, J., & Mayer, H. (2011). Impacts of street design parameters on human-biometeorological variables. *Meteorologische Zeitschrift*, *20*(5), 541–552. https://doi.org/10.1127/0941-2948/2011/0254

Hondula, D. M., Balling, R. C., Andrade, R., Scott Krayenhoff, E., Middel, A., Urban, A., … Sailor, D. J. (2017). Biometeorology for cities. *International Journal of Biometeorology*, *61*, 59–69. https://doi.org/10.1007/s00484-017-1412-3

Howell, J. R. (1982). *A catalog of radiation configuration factors*. McGraw-Hill Book Company.

Huang, H., Ooka, R., & Kato, S. (2005). Urban thermal environment measurements and numerical simulation for an actual complex urban area covering a large district heating and cooling system in summer. *Atmospheric Environment*, *39*(34), 6362–6375. https://doi.org/10.1016/j.atmosenv.2005.07.018

Huang, J., Cedeño-Laurent, J. G., & Spengler, J. D. (2014). CityComfort+: A simulation-based method for predicting mean radiant temperature in dense urban areas. *Building and Environment*, *80*, 84–95. https://doi.org/10.1016/j.buildenv.2014.05.019

Iio, A., Kakubari, Y., & Mizunaga, H. (2011). A three-dimensional light transfer model based on the vertical point-quadrant method and Monte-Carlo simulation in a Fagus crenata forest canopy on Mount Naeba in Japan. *Agricultural and Forest Meteorology*, *151*(4), 461–479. https://doi.org/10.1016/j.agrformet.2010.12.003

Jamei, E., & Rajagopalan, P. (2017). Urban development and pedestrian thermal comfort in Melbourne. *Solar Energy*, *144*, 681–698. https://doi.org/10.1016/j.solener.2017.01.023

Järvi, L., Grimmond, C. S. B., & Christen, A. (2011). The Surface Urban Energy and Water Balance Scheme (SUEWS): Evaluation in Los Angeles and Vancouver. *Journal of Hydrology*, *411*(3–4), 219–237. https://doi.org/10.1016/j.jhydrol.2011.10.001

Johansson, E., & Emmanuel, R. (2006). The influence of urban design on

outdoor thermal comfort in the hot, humid city of Colombo, Sri Lanka. *International Journal of Biometeorology*, *51*(2), 119–133. https://doi.org/10.1007/s00484-006-0047-6

Jones, D. F., Mirrazavi, S. K., & Tamiz, M. (2002). Multi-objective meta-heuristics: An overview of the current state-of-the-art. *IEuropean Journal of Operational Research*, *137*, 1–9. https://doi.org/10.1016/j.vlsi.2003.12.003

Kántor, N., Chen, L., & Gál, C. V. (2018). Human-biometeorological significance of shading in urban public spaces—Summertime measurements in Pécs, Hungary. *Landscape and Urban Planning*, *170*(September 2017), 241–255. https://doi.org/10.1016/j.landurbplan.2017.09.030

Kántor, N., Gál, C. V., Gulyás, Á., & Unger, J. (2018). The Impact of Façade Orientation and Woody Vegetation on Summertime Heat Stress Patterns in a Central European Square: Comparison of Radiation Measurements and Simulations. *Advances in Meteorology*, *2018*, 1–15. https://doi.org/10.1155/2018/2650642

Ketterer, C., & Matzarakis, A. (2014). Human-biometeorological assessment of heat stress reduction by replanning measures in Stuttgart, Germany. *Landscape and Urban Planning*, *122*, 78–88. https://doi.org/10.1016/j.landurbplan.2013.11.003

Klemm, W., Heusinkveld, B. G., Lenzholzer, S., & van Hove, B. (2015). Street greenery and its physical and psychological impact on thermal comfort. *Landscape and Urban Planning*, *138*, 87–98. https://doi.org/10.1016/j.landurbplan.2015.02.009

Konarska, J., Lindberg, F., Larsson, A., Thorsson, S., & Holmer, B. (2014). Transmissivity of solar radiation through crowns of single urban trees-application for outdoor thermal comfort modelling. *Theoretical and Applied Climatology*, *117*(3–4), 363–376. https://doi.org/10.1007/s00704-013-1000-3

Konarska, J., Uddling, J., Holmer, B., Lutz, M., Lindberg, F., Pleijel, H., & Thorsson, S. (2016). Transpiration of urban trees and its cooling effect in a high latitude city. *International Journal of Biometeorology*, *60*(1), 159–172. https://doi.org/10.1007/s00484-015-1014-x

Kong, F., Yin, H., James, P., & He, H. S. (2014). Effects of spatial pattern

of greenspace on urban cooling in a large metropolitan area of eastern China. *Landscape and Urban Planning*, *128*, 35–47. https://doi.org/10.1016/j.landurbplan.2014.04.018

Kong, L., Lau, K. K. L., Yuan, C., Chen, Y., Xu, Y., Ren, C., & Ng, E. (2017). Regulation of outdoor thermal comfort by trees in Hong Kong. *Sustainable Cities and Society*, *31*, 12–25. https://doi.org/10.1016/j.scs.2017.01.018

Krayenhoff, E. S., Christen, A., Martilli, A., & Oke, T. R. (2014). A Multi-layer Radiation Model for Urban Neighbourhoods with Trees. *Boundary-Layer Meteorology*, *151*(1), 139–178. https://doi.org/10.1007/s10546-013-9883-1

Krayenhoff, E. Scott, Moustaoui, M., Broadbent, A. M., Gupta, V., & Georgescu, M. (2018). Diurnal interaction between urban expansion, climate change and adaptation in US cities. *Nature Climate Change*, *8*(12), 1097–1103. https://doi.org/10.1038/s41558-018-0320-9

Krayenhoff, E. Scott, & Voogt, J. A. (2010). Impacts of urban albedo increase on local air temperature at daily-annual time scales: Model results and synthesis of previous work. *Journal of Applied Meteorology and Climatology*, *49*(8), 1634–1648. https://doi.org/10.1175/2010JAMC2356.1

Krayenhoff, E S, Santiago, J., Martilli, A., Christen, A., & Oke, T. R. (2015). Parametrization of Drag and Turbulence for Urban Neighbourhoods with Trees. *Boundary-Layer Meteorology*, *156*, 157–189. https://doi.org/10.1007/s10546-015-0028-6

Lee, H., Holst, J., & Mayer, H. (2013). Modification of human-biometeorologically significant radiant flux densities by shading as local method to mitigate heat stress in summer within urban street canyons. *Advances in Meteorology*, 1–13. https://doi.org/10.1155/2013/312572. article id 312572

Lee, H., & Mayer, H. (2016). Validation of the mean radiant temperature simulated by the RayMan software in urban environments. *International Journal of Biometeorology*, *60*(11), 1775–1785. https://doi.org/10.1007/s00484-016-1166-3

Lee, H., & Mayer, H. (2018a). Maximum extent of human heat stress reduction on building areas due to urban greening. *Urban Forestry and*

Urban Greening, *32*, 154–167. https://doi.org/10.1016/j.ufug.2018.04.010

Lee, H., & Mayer, H. (2018b). Thermal comfort of pedestrians in an urban street canyon is affected by increasing albedo of building walls. *International Journal of Biometeorology*, *62*(7), 1199–1209. https://doi.org/10.1007/s00484-018-1523-5

Lee, H., Mayer, H., & Chen, L. (2016). Contribution of trees and grasslands to the mitigation of human heat stress in a residential district of Freiburg, Southwest Germany. *Landscape and Urban Planning*, *148*(October 2017), 37–50. https://doi.org/10.1016/j.landurbplan.2015.12.004

Lee, H., Mayer, H., & Kuttler, W. (2018). To what extent does the air flow initialisation of the ENVI-met model affect human heat stress simulated in a common street canyon? *International Journal of Biometeorology*, *63*, 73–81. https://doi.org/10.1007/s00484-018-1637-9

Lee, H., Mayer, H., & Schindler, D. (2014). Importance of 3-D radiant flux densities for outdoor human thermal comfort on clear-sky summer days in Freiburg, Southwest Germany. *Meteorologische Zeitschrift*, *23*(3), 315–330. https://doi.org/10.1127/0941-2948/2014/0536

Li, D., Bou-Zeid, E., & Oppenheimer, M. (2014). The effectiveness of cool and green roofs as urban heat island mitigation strategies. *Environmental Research Letters*, *9*(5), 055002. https://doi.org/10.1088/1748-9326/9/5/055002

Lin, T. P. (2009). Thermal perception, adaptation and attendance in a public square in hot and humid regions. *Building and Environment*, *44*(10), 2017–2026. https://doi.org/10.1016/j.buildenv.2009.02.004

Lindberg, F., & Grimmond, C. S. B. (2011). Nature of vegetation and building morphology characteristics across a city: Influence on shadow patterns and mean radiant temperatures in London. *Urban Ecosystems*, *14*(4), 617–634. https://doi.org/10.1007/s11252-011-0184-5

Lindberg, F., Holmer, B., & Thorsson, S. (2008). SOLWEIG 1.0 - Modelling spatial variations of 3D radiant fluxes and mean radiant temperature in complex urban settings. *International Journal of Biometeorology*, *52*(7), 697–713. https://doi.org/10.1007/s00484-008-

0162-7

Lobaccaro, G., & Acero, J. A. (2015). Comparative analysis of green actions to improve outdoor thermal comfort inside typical urban street canyons. *Urban Climate*, *14*, 251–267. https://doi.org/10.1016/j.uclim.2015.10.002

Macro, K., Matott, L. S., Rabideau, A., Ghodsi, S. H., & Zhu, Z. (2019). OSTRICH-SWMM: A new multi-objective optimization tool for green infrastructure planning with SWMM. *Environmental Modelling and Software*, *113*(November 2018), 42–47. https://doi.org/10.1016/j.envsoft.2018.12.004

Maria Raquel, C. de S., Montalto, F. A., & Palmer, M. I. (2016). Potential climate change impacts on green infrastructure vegetation. *Urban Forestry and Urban Greening*, *20*, 128–139. https://doi.org/10.1016/j.ufug.2016.08.014

Martilli, A., Clappier, A., & Rotach, M. W. (2002). An urban surface exchange parameterisation for mesoscale models. *Boundary-Layer Meteorology*, *104*(2), 261–304. https://doi.org/10.1023/A:1016099921195

Matzarakis, A., Rutz, F., & Mayer, H. (2010). Modelling radiation fluxes in simple and complex environments: Basics of the RayMan model. *International Journal of Biometeorology*, *54*(2), 131–139. https://doi.org/10.1007/s00484-009-0261-0

Mayer, H., Holst, J., Dostal, P., Imbery, F., & Schindler, D. (2008). Human thermal comfort in summer within an urban street canyon in Central Europe. *Meteorologische Zeitschrift*, *17*(3), 241–250. https://doi.org/10.1127/0941-2948/2008/0285

Middel, A., & Krayenhoff, E. S. (2019). Micrometeorological determinants of pedestrian thermal exposure during record-breaking heat in Tempe , Arizona : Introducing the MaRTy observational platform. *Science of the Total Environment*, *687*, 137–151. https://doi.org/10.1016/j.scitotenv.2019.06.085

Mohammadi, M., Nastaran, M., & Sahebgharani, A. (2016). Development, application, and comparison of hybrid meta-heuristics for urban land-use allocation optimization: Tabu search, genetic, GRASP, and simulated annealing algorithms. *Computers, Environment and Urban*

Systems, *60*, 23–36. https://doi.org/10.1016/j.compenvurbsys.2016.07.009

Morakinyo, T. E., & Lam, Y. F. (2016). Simulation study on the impact of tree-configuration, planting pattern and wind condition on street-canyon's micro-climate and thermal comfort. *Building and Environment*, *103*, 262–275. https://doi.org/10.1016/j.buildenv.2016.04.025

Nakamura, Y., & Oke, T. R. (1988). Wind, temperature and stability conditions in an east-west oriented urban canyon. *Atmospheric Environment*, *22*, 2691–2700. https://doi.org/10.1016/0004-6981(88)90437-4

Napoli, M., Massetti, L., Brandani, G., Petralli, M., & Orlandini, S. (2016). Modeling tree shade effect on urban ground surface temperature. *Journal of Environmental Quality*, *45*(1), 146–156.

Norton, B. a., Coutts, A. M., Livesley, S. J., Harris, R. J., Hunter, A. M., & Williams, N. S. G. (2015). Planning for cooler cities: A framework to prioritise green infrastructure to mitigate high temperatures in urban landscapes. *Landscape and Urban Planning*, *134*, 127–138. https://doi.org/10.1016/j.landurbplan.2014.10.018

Ohashi, Y., Ihara, T., Kikegawa, Y., & Sugiyama, N. (2016). Numerical simulations of influence of heat island countermeasures on outdoor human heat stress in the 23 wards of Tokyo, Japan. *Energy and Buildings*, *114*, 104–111. https://doi.org/10.1016/j.enbuild.2015.06.027

Oliveira, S., Andrade, H., & Vaz, T. (2011). The cooling effect of green spaces as a contribution to the mitigation of urban heat: A case study in Lisbon. *Building and Environment*, *46*(11), 2186–2194. https://doi.org/10.1016/j.buildenv.2011.04.034

Oudin Åström, D., Forsberg, B., Ebi, K. L., & Rocklöv, J. (2013). Attributing mortality from extreme temperatures to climate change in Stockholm, Sweden. *Nature Climate Change*, *3*(12), 1050–1054. https://doi.org/10.1038/nclimate2022

Overby, M., Willemsen, P., Bailey, B. N., Halverson, S., & Pardyjak, E. R. (2016). A rapid and scalable radiation transfer model for complex urban domains. *Urban Climate*, *15*, 25–44. https://doi.org/10.1016/j.uclim.2015.11.004

Park, C. Y., Lee, D. K., Krayenhoff, E. S., Heo, H. K., Ahn, S., Asawa, T., … Kim, H. G. (2018). A multilayer mean radiant temperature model for pedestrians in a street canyon with trees. *Building and Environment*, *141*, 298–309. https://doi.org/10.1016/j.buildenv.2018.05.058

Park, W., Kang, G., Park, J., Lee, S., & Song, D. (2012). Calculation Method of Indoor Solar Heat Gain in Building Envelope with Shading Device. In *The Society of Air-Conditioning and Refrigerating Engineers of Korea* (pp. 155–161).

Peterson, G. D., Cumming, G. S., & Carpenter, S. R. (2003). Scenario Planning: a Tool for Conservation in an Uncertain World. *Conservation Biology*, *17*(2), 358–366.

Qin, Y., & He, H. (2017). A new simplified method for measuring the albedo of limited extent targets. *Solar Energy*, *157*, 1047–1055. https://doi.org/10.1016/j.solener.2017.09.027

Rahman, M. A., Moser, A., Gold, A., Rötzer, T., & Pauleit, S. (2018). Vertical air temperature gradients under the shade of two contrasting urban tree species during different types of summer days. *Science of The Total Environment*, *633*, 100–111. https://doi.org/10.1016/j.scitotenv.2018.03.168

Rahman, M. A., Moser, A., Rötzer, T., & Pauleit, S. (2017). Microclimatic differences and their influence on transpirational cooling of Tilia cordata in two contrasting street canyons in Munich, Germany. *Agricultural and Forest Meteorology*, *232*, 443–456. https://doi.org/10.1016/j.agrformet.2016.10.006

Ramírez, A. Z., & Muñoz, C. B. (2012). *Albedo Effect and Energy Efficiency of Cities, Sustainable Development – Energy, Engineering and Technologies – Manufacturing and Environment* (Manufacturing and Environment, Prof. Chaouki Ghenai (Ed.),). Manufacturing and Environment, Prof. Chaouki Ghenai (Ed.),. https://doi.org/10.5772/29536

Redon, E., Lemonsu, A., Masson, V., Morille, B., & Musy, M. (2016). Implementation of street trees in solar radiative exchange parameterization of TEB in SURFEX v8.0. *Geoscientific Model Development Discussions*, (August), 1–46. https://doi.org/10.5194/gmd-2016-157

Richard, C., Doré, G., Lemieux, C., Bilodeau, J.-P., & Haure-touzé, J. (2015). Albedo of Pavement Surfacing Materials : In Situ Measurements. *Cold Regions Engineering*, 181–193. https://doi.org/10.1061/9780784479315.017

Rizwan, A. M., Dennis, L. Y. C., & Liu, C. (2008). A review on the generation, determination and mitigation of Urban Heat Island. *Journal of Environmental Sciences*, *20*, 120–128. https://doi.org/10.1016/S1001-0742(08)60019-4

Rosso, F., Golasi, I., Castaldo, V. L., Piselli, C., Pisello, A. L., Salata, F., … de Lieto Vollaro, A. (2018). On the impact of innovative materials on outdoor thermal comfort of pedestrians in historical urban canyons. *Renewable Energy*, *118*, 825–839. https://doi.org/10.1016/j.renene.2017.11.074

Ryu, Y. H., Bou-Zeid, E., Wang, Z. H., & Smith, J. A. (2016). Realistic Representation of Trees in an Urban Canopy Model. *Boundary-Layer Meteorology*, *159*(2), 193–220. https://doi.org/10.1007/s10546-015-0120-y

Salata, F., Golasi, I., Vollaro, A. D. L., & Vollaro, R. D. L. (2015). How high albedo and traditional buildings' materials and vegetation affect the quality of urban microclimate. A case study. *Energy and Buildings*, *99*, 32–49. https://doi.org/10.1016/j.enbuild.2015.04.010

Scott Krayenhoff, E., & Voogt, J. A. (2016). Daytime thermal anisotropy of urban neighbourhoods: Morphological causation. *Remote Sensing*, *8*(2), 1–22. https://doi.org/10.3390/rs8020108

Shahidan, M. F., Jones, P. J., Gwilliam, J., & Salleh, E. (2012). An evaluation of outdoor and building environment cooling achieved through combination modification of trees with ground materials. *Building and Environment*, *58*, 245–257. https://doi.org/10.1016/j.buildenv.2012.07.012

Shashua-bar, L., & Hoffman, M. E. (2000). Vegetation as a climatic component in the design of an urban street An empirical model for predicting the cooling effect of urban green areas with trees. *Energy and Buildings*, *31*, 221–235. https://doi.org/10.1016/S0378-7788(99)00018-3

Shashua-Bar, L., Tsiros, I. X., & Hoffman, M. E. (2010). A modeling study

for evaluating passive cooling scenarios in urban streets with trees. Case study: Athens, Greece. *Building and Environment*, *45*(12), 2798–2807. https://doi.org/10.1016/j.buildenv.2010.06.008

Shashua-bar, Limor, & Hoffman, M. E. (2003). Geometry and orientation aspects in passive cooling of canyon streets with trees. *Energy and Buildings*, *35*(1), 61–68.

Shashua-bar, Limor, Tsiros, I. X., & Hoffman, M. (2012). Passive cooling design options to ameliorate thermal comfort in urban streets of a Mediterranean climate (Athens) under hot summer conditions. *Building and Environment*, *57*, 110–119. https://doi.org/10.1016/j.buildenv.2012.04.019

Stewart, I. D., & Oke, T. R. (2012). Local climate zones for urban temperature studies. *Bulletin of the American Meteorological Society*, *93*(12), 1879–1900. https://doi.org/10.1175/BAMS-D-11-00019.1

Sun, C.-Y. (2011). A street thermal environment study in summer by the mobile transect technique. *Theoretical and Applied Climatology*, *106*(3–4), 433–442. https://doi.org/10.1007/s00704-011-0444-6

Sun, R., Chen, A., Chen, L., & Lü, Y. (2012). Cooling effects of wetlands in an urban region: The case of Beijing. *Ecological Indicators*, *20*, 57–64. https://doi.org/10.1016/j.ecolind.2012.02.006

Takebayashi, H., Kimura, Y., & Kyogoku, S. (2014). Study on the appropriate selection of urban heat island measure technologies to urban block properties. *Sustainable Cities and Society*, *13*, 217–222. https://doi.org/10.1016/j.scs.2014.01.008

Takebayashi, H., & Moriyama, M. (2009). Study on the urban heat island mitigation effect achieved by converting to grass-covered parking. *Solar Energy*, *83*(8), 1211–1223. https://doi.org/10.1016/j.solener.2009.01.019

Taleghani, M., Sailor, D. J., Tenpierik, M., & van den Dobbelsteen, A. (2014). Thermal assessment of heat mitigation strategies: The case of Portland State University, Oregon, USA. *Building and Environment*, *73*, 138–150. https://doi.org/10.1016/j.buildenv.2013.12.006

Taleghani, M., Tenpierik, M., Dobbelsteen, A. Van Den, & Sailor, D. J. (2014). Heat in courtyards: A validated and calibrated parametric study of heat mitigation strategies for urban courtyards in the Netherlands.

Solar Energy, *103*, 108–124. https://doi.org/10.1016/j.solener.2014.01.033

Thorsson, S., Lindberg, F., Eliasson, I., & Holmer, B. (2007). Different methods for estimating the mean radiant temperature in an outdoor urban setting. *International Journal of Climatology*, *27*, 1983–1993. https://doi.org/10.1002/joc.1537

Thorsson, S., Rocklöv, J., Konarska, J., Lindberg, F., Holmer, B., Dousset, B., & Rayner, D. (2014). Mean radiant temperature - A predictor of heat related mortality. *Urban Climate*, *10*, 332–345. https://doi.org/10.1016/j.uclim.2014.01.004

Tominaga, Y., Sato, Y., & Sadohara, S. (2015). CFD simulations of the effect of evaporative cooling from water bodies in a micro-scale urban environment: Validation and application studies. *Sustainable Cities and Society*, *19*, 259–270. https://doi.org/10.1016/j.scs.2015.03.011

Wang, J., Huang, B., Fu, D., & Atkinson, P. (2015). Spatiotemporal Variation in Surface Urban Heat Island Intensity and Associated Determinants across Major Chinese Cities. *Remote Sensing*, *7*, 3670–3689. https://doi.org/10.3390/rs70403670

Wang, M., Chang, H. C., Merrick, J. R., & Amati, M. (2016). Assessment of solar radiation reduction from urban forests on buildings along highway corridors in Sydney. *Urban Forestry and Urban Greening*, *15*, 225–235. https://doi.org/10.1016/j.ufug.2016.01.003

Wang, Z.-H. (2014). Monte Carlo simulations of radiative heat exchange in a street canyon with trees. *Solar Energy*, *110*, 704–713. https://doi.org/10.1016/j.solener.2014.10.012

Wondmagegn, B. Y., Xiang, J., Williams, S., Pisaniello, D., & Bi, P. (2019). What do we know about the healthcare costs of extreme heat exposure? A comprehensive literature review. *Science of the Total Environment*, *657*, 608–618. https://doi.org/10.1016/j.scitotenv.2018.11.479

Woodward, M., Kapelan, Z., & Gouldby, B. (2014). Adaptive flood risk management under climate change uncertainty using real options and optimization. *Risk Analysis*, *34*(1), 75–92. https://doi.org/10.1111/risa.12088

Wu, W., Maier, H. R., Dandy, G. C., Leonard, R., Bellette, K., Cuddy, S., & Maheepala, S. (2016). Including stakeholder input in formulating and

solving real-world optimisation problems: Generic framework and case study. *Environmental Modelling and Software*, *79*, 197–213. https://doi.org/10.1016/j.envsoft.2016.02.012

Wu, Z., & Chen, L. (2017). Optimizing the spatial arrangement of trees in residential neighborhoods for better cooling effects: Integrating modeling with in-situ measurements. *Landscape and Urban Planning*, *167*, 463–472. https://doi.org/10.1016/j.landurbplan.2017.07.015

Xuan, Y., Yang, G., Li, Q., & Mochida, A. (2016). Outdoor thermal environment for different urban forms under summer conditions, 281–296. https://doi.org/10.1007/s12273-016-0274-7

Yang, J., Wang, Z. H., & Kaloush, K. E. (2015). Environmental impacts of reflective materials: Is high albedo a "silver bullet" for mitigating urban heat island? *Renewable and Sustainable Energy Reviews*, *47*, 830–843. https://doi.org/10.1016/j.rser.2015.03.092

Yoon, E. J., Kim, B., & Lee, D. K. (2019). Multi-objective planning model for urban greening based on optimization algorithms. *Urban Forestry & Urban Greening*, 1–12. https://doi.org/10.1016/j.ufug.2019.01.004

Yuan, J., Emura, K., & Farnham, C. (2017). Is urban albedo or urban green covering more effective for urban microclimate improvement?: A simulation for Osaka. *Sustainable Cities and Society*, *32*, 78–86. https://doi.org/10.1016/j.scs.2017.03.021

Zardo, L., Geneletti, D., Pérez-soba, M., & Eupen, M. Van. (2017). Estimating the cooling capacity of green infrastructures to support urban planning. *Ecosystem Services*, *26*, 225–235. https://doi.org/10.1016/j.ecoser.2017.06.016

Zeng, Y. L., & Dong, L. (2015). Thermal human biometeorological conditions and subjective thermal sensation in pedestrian streets in Chengdu, China. *International Journal of Biometeorology*, *59*(1), 99–108. https://doi.org/10.1007/s00484-014-0883-8

Zölch, T., Maderspacher, J., Wamsler, C., & Pauleit, S. (2016). Using green infrastructure for urban climate-proofing: An evaluation of heat mitigation measures at the micro-scale. *Urban Forestry and Urban Greening*, *20*, 305–316. https://doi.org/10.1016/j.ufug.2016.09.011

Zoras, S., Tsermentselis, A., Kosmopoulos, P., & Dimoudi, A. (2014). Evaluation of the application of cool materials in urban spaces: A case

study in the center of Florina. *Sustainable Cities and Society*, *13*, 223–229. https://doi.org/10.1016/j.scs.2014.01.007

국문 초록

보행로에서의 복사 노출 저감 평가 모델과 수목을 이용한 의사결정에 적용

박 채 연

서울대학교 대학원 협동과정 조경학
지도교수: 이 동 근

도시열섬과 기후변화로 인한 도시의 열 증가는 도시민의 건강을 위협하고 있다. 대부분의 보행로는 식재 등의 투수성 포장이 아닌 불투수성 표면으로 이루어져 있고, 자동차와 건물 등에서 인공열이 발생하기 때문에 열환경이 좋지 않다. 따라서 계획가들은 보행자의 열 스트레스를 낮추기 위한 열 완화 전략을 고려해야 한다. 특히나 열 스트레스는 공기 온도 이외에 도시 협곡의 복사열 환경에 크게 영향을 받기 때문에, 보행자 복사열 노출을 줄이기 위한 전략이 연구되어야 한다.

지금까지 복사열 노출을 막기 위한 여러 전략이 연구되어 왔는데, 그 중 가로수는 그늘 효과를 통해 보행자 복사열을 줄일 수 있는 효과적인 전략으로 알려져 있다. 그러나, 도시계획가와 같은 의사결정자는 그들의 결정에 의

해 얼마나 많은 복사열이 감소되는지 알지 못하며, 가장 효과적으로 복사열을 저감하는데 필요한 가로수의 설계 옵션이 무엇인지 알기가 어렵다. 따라서 본 연구는 가로수를 이용한 보행자 복사열 저감 계획을 지원해주는 의사결정 도구를 개발하는 것을 목표로 한다.

본 연구는 가로수와 건물의 디자인에 따라 변화되는 보행자의 복사열을 추정할 수 있는 모델을 개발했다. 이 모델은 각 도시 요소 및 형태 계수를 통해 단파 및 장파 복사 교환을 모의한 후 보행자의 평균 복사 온도를 계산한다. 이러한 평가 모델을 활용하여, 본 연구에서는 첫 번째로 가로수 설계 변수인 나무 크기와 식재 간격에 따라 달라지는 평균복사온도를 확인하였다. 나무 간격이 감소할수록 작은 나무에서 평균복사온도 감소가 기하 급수적으로 증가하는 것을 밝혀냈다. 의사결정자는 위와 같은 결과를 바탕으로 그들이 선택한 설계 변수가 가질 복사열 저감 효과를 파악할 수 있을 것이다.

실제 보행로에는 가로수 외에 다양한 복사열 저감 전략이 적용될 수 있다. 이러한 현실 문제를 반영하기 위하여, 본 연구에서는 의사결정 지원 모델 중 하나로 다중 전략 조합 모델을 제안했다. 나무, 잔디, 건물 벽 및 보행로의 알베도 감소로 구성된 전략 중 효과적인 구성을 찾기 위해서, 평균

복사온도를 최대로 저감하고 비용을 최소로 하는 것을 목적함수로 설정하였다. 이 모델은 두 가지 목적함수를 만족시키는 다양한 옵션을 제공함으로써 의사결정자가 그들의 선호도나 대상지 특성에 맞는 계획안을 선택할 수 있도록 하였다.

본 연구는 가로수 설계 변수에 따른 복사열 저감과 비용-효과적인 전략들의 조합을 제공함으로써 가장 효율적인 가로수 설계가 가능하도록 하는 의사결정 지원도구를 제안한다. 위 도구는 가로수를 이용하여 보행로의 열환경을 개선함으로써 지속가능한 도시 계획에 대한 통찰력을 제공할 것이다.

주요어: 도시열섬, 식재계획, 평균복사온도, 최적화, 그림자 효과

학번: 2017-37831

APPENDICES

Appendix A. A multilayer mean radiant temperature model for pedestrians in a street canyon with trees

Table A. 1. Model parameters

Classes	Description	Symbol	Default	Units/(type)
Input data	Date and time			
	Date	-		DOY
	Time	-		H
	Latitude and longitude			
	Latitude	-		°
	Longitude	-		°
	Meteorological data			
	Air temperature	T_a	-	K
	Dewpoint temperature	TempDew	-	K
	Cloud fraction	cf	0-1	-
	Wind speed	v_{wind}	-	m/s
	Geometric data			
	Street orientation	χ	0-360	Radian
	Building probability density profile	B, SB	-	(matrix)
	Roof probability density profile	R	-	(matrix)
	Tree LAD profile	T	-	(matrix)
	Building width	Xb	-	m
	Sidewalk width	Xw	-	m
	Road width	Xr	-	m
	Tree crown width	cw	5	m
	Tree trunk height	ch	5	m
	Pedestrian height	p	2	m
	Vertical layer thickness (building)	Δz	5	m
	Vertical layer thickness (tree)	Δzt	1	m
	Vertical layer index (building, tree)	iz	-	-
	Number of vertical layers (building, tree)	-	10	-
Computational parameters	Index of rays	i	-	-
	Number of rays	ni	10,000	-

	Index of ray steps	j	-	-
	Number of ray steps	nj	-	-
	Ray step size (view factor)	Δs	1	m
	Ray step size (direct shortwave radiation)	$\Delta s'$	0.1	m
Radiative parameters	Albedo of walls	αB	0.4	-
	Albedo of roofs	αR	0.15	-
	Albedo of sidewalks	αW	0.2	-
	Albedo of roads	αR	0.1	-
	Albedo of trees	αT	0.18	-
	Emissivity of walls	εB	0.9	-
	Emissivity of roofs	εR	0.9	-
	Emissivity of sidewalks	εW	0.95	-
	Emissivity of roads	εR	0.95	-
	Emissivity of trees	εT	0.96	-
Radiation environments	Solar zenith angle	θ	-	Radian
	Solar azimuth angle	φ	-	Radian
	Global shortwave radiation	K	-	W/m²
	Extraterrestrial shortwave radiation	K^O	-	W/m²
	Clearness index	K^T	0-1	-
	Direct shortwave radiation	K_{dir}	--	W/m²
	Diffuse shortwave radiation	K_{dif}	-	W/m²
	Net shortwave radiation of element *E(iz)*	*KE(iz)*	-	W/m²
	Upward shortwave radiation from element *E(iz)*	$K_{up}E(iz)$	-	W/m²
	Total incident shortwave radiation on element *E(iz)*	$K_{down}E(iz)$	-	W/m²
	Longwave irradiance from the sky	L^{sky}	-	W/m²
	Net longwave radiation of element *E(iz)*	*LE(iz)*	-	W/m²
	Upward longwave radiation from element *E(iz)*	$L_{up}E(iz)$	-	W/m²
	Total incident longwave radiation on element *E(iz)*	$L_{down}E(iz)$	-	W/m²
	Area weighted view factor from *E(iz)* to *E'(iz)*	$F_{E(iz)\to E'(iz)}$		-
	Surface temperature of walls	*TB, TSB*		K (matrix)
	Surface temperature of roofs	*TR*		K (matrix)
	Surface temperature of sidewalks	*TW*		K

	Surface temperature of roads	*TR*		K
	Surface temperature of trees	*TV*		K (matrix)

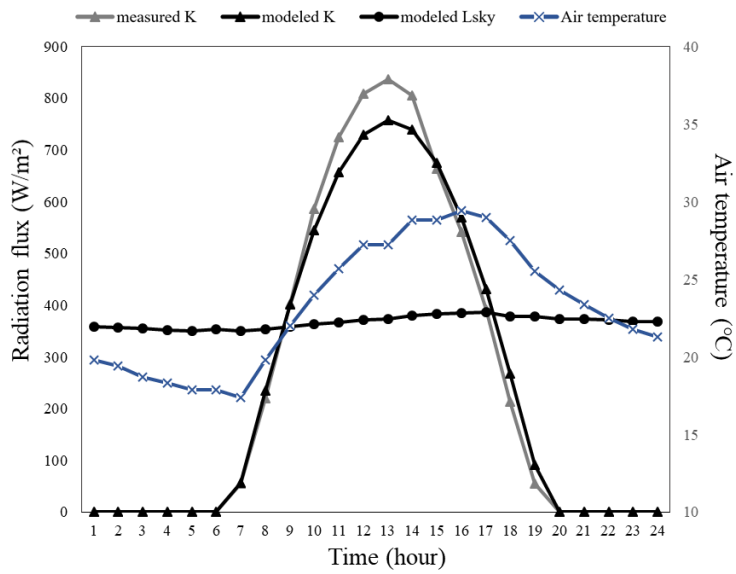

Fig. A. 1. Global radiation flux on 244 DOY, 2017. *K* (global shortwave radiation), modeled *Lsky* (global longwave radiation), and air temperature.

Appendix B. Variations in pedestrian mean radiant temperature based on the spacing and size of street trees

In order to valid the tree's effect of the MMRT model, this study compared the simulation result with measured MRT. The validation site was Dongyo-ro, Mapo-gu, Seoul which relates to our model setup. The geometry of the validation site has 20 m wide road with 20 m long buildings and 5 m wide sidewalk, and the h/w is 0.67. The orientation of the study site is over 70 °. The measurement time was 1000-1500 LST, 25th September, 2018. For MRT measurement, this study used 6 direction radiometers (used three CNR4 net radiometers (Keipp & Zonen, CNR4). I measured MRT while I was walking through a street. This study calculated mean MRT of each street.

Fig. A. 2. The study site of MMRT validation.

For model simulations, the input variables in the Table A.2 were used. This study used measured air temperature, and wind speed, and downward solar radiation in the model.

Table A. 2. The input variables for model simulation.

	Street 1		Street 2		Street 3	
	S-facing	N-facing	S-facing	N-facing	S-facing	N-facing
LAD X w/x	0.41	0.36	0.63	0.44	0.67	0.58
Tree height (m)	7	7	7	8	9	9
Street orientation (°)	70	70	75	75	80	80
Building height (m)	20	20	20	20	20	20
Building wall albedo	0.4	0.4	0.4	0.4	0.4	0.4
Road width (m)	20	20	20	20	20	20
Road albedo	0.1	0.1	0.1	0.1	0.1	0.1
Sidewalk width (m)	5	5	5	5	5	5
Sidewalk albedo	0.2	0.2	0.2	0.2	0.2	0.2

This study used R^2 and RMSE as for comparing measured (M) and estimated (E) MRT. R^2 and RMSE were computed as follows:

$$R^2 = 1 - \frac{\sum(E_i - M_i)^2}{\sum(E_i - M_{mean})^2}$$

$$\text{RMSE} = \left(\frac{1}{n}\sum(E_i - M_i)^2\right)^{1/2}$$

When compared the model value and measurement MRT, R^2 was 0.9 and RMSE was 11.9 K. The result indicates the simulation model sufficiently reflect the real world and consider shading effect. The model validation should be continued in the various sites.

Appendix C. Optimal multi-strategies modeling reveals a range of options for reducing pedestrian radiation exposure that integrate four strategies

Table A. 3. Albedo ranges for sidewalks and building walls obtained from previous studies (Hendel, Parison, Grados, & Royon, 2018; Qin & He, 2017; Ramírez & Muñoz, 2012; Salata et al., 2015; Shahidan et al., 2012).

	high ←———————————————————————————					
Sidewalk	Polished white granite (0.8)	Portland cement concrete (0.7–0.8)	White granite (0.65)	Ceramics (0.42)	Stabilized sand (0.4)	Portland cement concrete (0.35–0.4)
Wall	white paint (0.5–0.9),				Stone (0.4)	
	———————————————————————————→ low					
Sidewalk	Granite (0.3)	Limestone block (0.27)	Asphalt (0.2–0.05)	Wood tile (0.17)	Highly mottled concrete, dark brick (0.1)	
Wall			Brick (0.2)			

This study chose the population size and number of iterations using a repetitive pilot test. First, this study increased the population size to 50, 70, and 100 with enough iterations (100) and confirmed the shape of the Pareto optimality. The results showed no substantial difference between the three Pareto optimality values and that a population size of 70 was sufficient. Second, this study compared the results by increasing the number of iterations (1–100) with a population size of 70. This study confirmed the maximum or minimum values of the objectives and the Pareto optimality shape. After 80 iterations, the Pareto optimality values did not increase and the maximum

benefit value and minimum cost value remained constant. Therefore, this study selected 80 as the number of iterations.

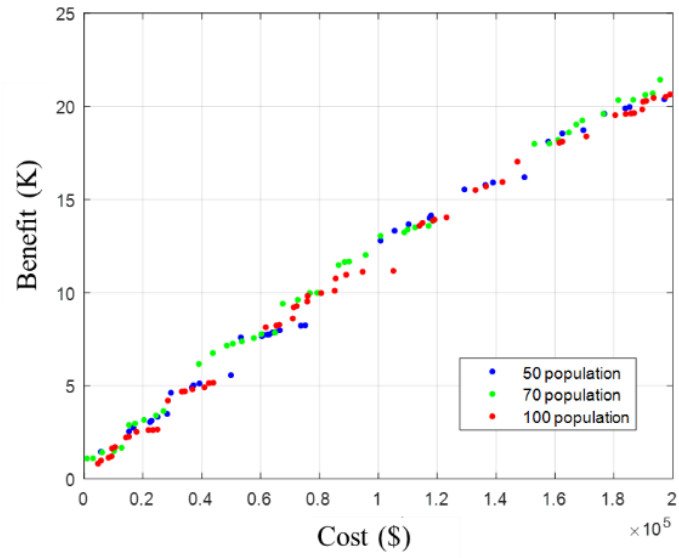

Fig. A. 3. Pareto optimality for different population sizes.

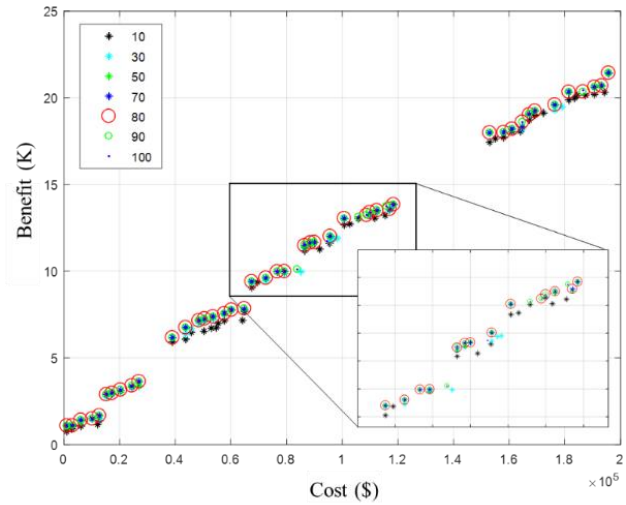

Fig. A. 4. Pareto optimality for different numbers of iterations (10, 30, 50, 70, 80, 90, 100).

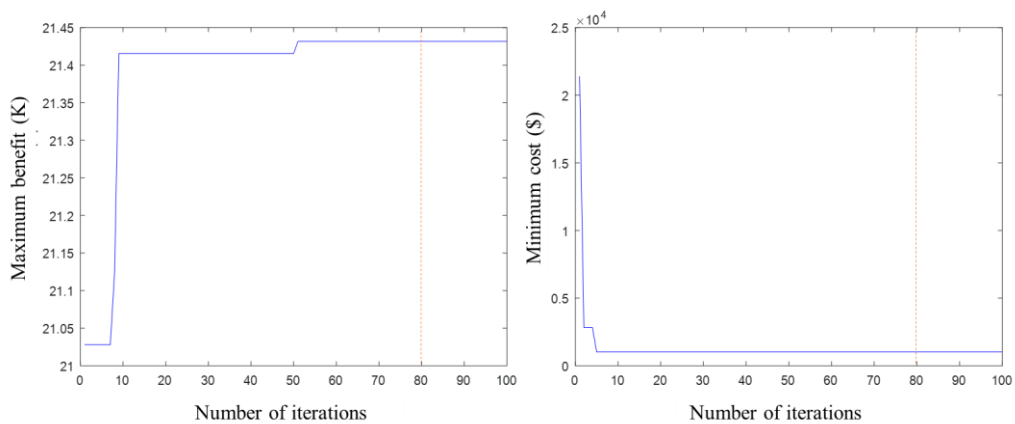

Fig. A. 5. Extreme values of the two objectives (benefit and cost).